XV. PLASMA ELECTRONICS*

Prof. L. D. Smullin
Prof. H. A. Haus
Prof. A. Bers
Prof. W. D. Getty
Prof. D. J. Rose
Prof. T. H. Dupree
Prof. L. M. Lidsky
Prof. E. P. Gyftopoulos
Dr. T. Musha
R. R. Bartsch
T. S. Brown
J. F. Clarke
J. A. Davis
F. E. Dunn
P. H. Edmonds
S. A. Evans
T. J. Fessenden
R. W. Flynn
F. Gardiol
E. T. Gerry
J. N. Hamawi
C-F. G. Hsi
G. I. Kachen, Jr.
C. A. Kapetanakos
B. R. Kusse
S. H. Kyong
M. A. Lieberman
M. Lind
M. D. Lubin
J. D. Mills
R. W. Moir
A. A. Offenberger
K. C. Papadopoulos
R. R. Parker
L. M. Petrie, Jr.
C. S. Ribbeck
H. M. Schneider
E. Thompson
C. E. Wagner
R. N. Wallace
J. C. Woo

RESEARCH OBJECTIVES

1. Plasmas for Electrical Energy Conversion

The work of this group is best understood in terms of the rationale behind the experimental and theoretical program. We are interested, primarily, in contributing to the ultimate development of a controlled thermonuclear reactor for power generation. Our primary problem, of course, is the production of a dense, hot, and stable plasma, well-insulated from the surrounding vacuum wall. A variety of schemes for generating such a plasma is under active study in many laboratories. An interesting way of comparing them is in terms of the order in which the major components are assembled. These components are: the vacuum wall, the magnetic field, the neutral gas or the plasma itself. The vacuum wall is always "assembled" first; the order of assembly of the magnetic field and plasma is arbitrary.

In the Θ-pinch the vacuum wall and gas are assembled first, then the magnetic field is rapidly built up, thereby feeding energy into the plasma and confining it, too.

In the DCX, Alice, and Stellerator, essentially steady magnetic fields are used and the plasma is produced last. In the DCX and Alice the plasma is assembled by injecting energetic ions (neutrals) that were accelerated in some external machine; it is hoped that these particles will be trapped in the magnetic mirror and thus build up a plasma.

We have chosen to study systems in which the cold, neutral gas and magnetic field are assembled first, and then energy is fed into the system to ionize the gas and heat the resulting plasma. The energy can be introduced in several ways, and we have chosen to study two methods: injection of high-frequency or microwave power, and injection of a high-power DC electron beam into the region to be ionized. The microwave power method is embodied in our electron-cyclotron-discharge experiments. The electron beam method is utilized in the beam-plasma discharge.

(a) Beam-Plasma Discharge

We have three machines in operation: Systems A, C, and D. System A is being used to study the details of the microwave interaction between the beam and the plasma. System C is being used to study methods of ion heating in a beam-plasma discharge, and to study the origin of the anomalously high-energy tail of the electron distribution. System D, which has just been put into operation, will be used for experiments with new

*This work was supported in part by the National Science Foundation (Grant GK-57).

and more powerful electron guns, and with its very strong magnetic field (up to 10 kgauss) it should begin to indicate some of the limits on plasma density and temperature that can be produced in a beam-plasma-discharge.

(b) Electron Cyclotron Discharge

We shall continue the study of the pulsed discharge and plan to terminate it in the summer of 1965.

A hybrid apparatus has been built to study beam interactions with plasmas whose electron temperature V_T is greater than the beam energy V_o. The plasma is a cyclotron discharge, energized by a 2400 Mc/sec cw magnetron. A low-voltage, low-power beam (100-500 ev) is used to probe the plasma. By modulating the injected beam at frequencies near ω_{pi} or ω_{ci}, it will be possible to study interactions between the beam and ion waves of various sorts.

The theoretical work of the group has been concerned primarily with the study of instabilities in plasmas and beam-plasma systems. With the aid of the facilities of Project MAC we now have a fairly complete system for the analysis and characterization of instabilities. Problems that are now under study are: beam-plasma instabilities in the vicinity of frequencies that are characteristics of the ions; beam-plasma interactions for beams injected across the magnetic field; instabilities in plasmas with mirror-type distribution functions. Other theoretical work is concerned with wave-propagation in bounded, warm plasma, various studies of active and passive waves in solid-state plasmas, and a study of non-adiabatic trapping in mirror fields where the magnetic moment cannot be considered as constant.

L. D. Smullin, A. Bers, W. D. Getty, T. Musha

2. Highly Ionized Plasma and Fusion Research

Studies that are applicable to controlled nuclear fusion assume many forms. Our activities, for the most part, are involved with plasmas: plasma kinetic theory, plasma production by injection, nonadiabatic particle motions, stability and turbulence, and interaction with coherent radiation. Our other activities (energy extraction and tritium regeneration through a surrounding blanket, superconducting magnetic-field structures for plasma confinement), while motivated by the thought of controlled fusion, have wider applicability.

(a) Plasma Properties of Laser Systems

A study is being made of the properties of various plasmas that exhibit laser action, with particular application to the hollow-cathode arc and to the generation of cw and pulsed laser radiation at high powers and with very low divergence. This will enable extension of techniques for photon-plasma interaction studies to different wavelengths and to a greater range of problems.

E. Thompson, P. H. Edmonds, L. M. Lidsky

(b) Plasma Kinetic Theory

Our research in plasma kinetic theory is concentrated in two general areas. The first is concerned with the derivation of "reasonably" simple but "reasonably" exact equations to provide a complete description of plasma behavior. The starting point has usually been a set of generalized hierarchy equations that includes the transverse electromagnetic field. The second phase of the program is directed toward obtaining interesting solutions to the fundamental equations to second order in the plasma parameter.

General formulas for the approach to equilibrium, including expressions for radiation emission and absorption, have been derived.

T. H. Dupree

(c) Hollow-Cathode Arc Properties

Investigation of the properties of the hollow-cathode arc continues to gain a more complete understanding of the mechanism of the arc and the properties of the plasma. Particular current studies are: (i) measurement of plasma temperatures by pulsed-probe methods, (ii) extraction and analysis of the various plasma constituents by time of flight and retarding potential-difference techniques. Additional information on the hollow-cathode discharge is being obtained from the laser-plasma interaction studies.

P. H. Edmonds, M. D. Lubin

(d) Superconducting Magnets and Components

A small sustaining program on the design of superconducting systems and components is being carried on to develop (i) supercon-supercon and supercon-normal connections for use in vacuum, (ii) heat-transfer and mechanical design criteria that are suitable for application to large magnets, and (iii) techniques for reassembly for a large magnet to avoid problems in our earlier design (chiefly helium leaks into the vacuum space).

P. H. Edmonds, L. M. Lidsky, D. J. Rose, S. A. Evans

(e) Thermonuclear System Engineering Studies

The first series of studies on a blanket for moderating 14 Mev D-T neutrons and regenerating tritium is virtually complete. The results show that a blanket is theoretically feasible, and that the calculations can be checked (very roughly) by experiments on a mock-up assembly. Further studies will concentrate on (i) development of Monte Carlo and other calculations for determining the neutron spectrum in finite assemblies subject to experimental check, and (ii) refinement of the experiments to measure actual tritium regeneration, as well as moderated neutrons.

Work will also continue to assess the chances of engineering and economic success for fusion power.

D. J. Rose, L. M. Petrie, Jr., F. E. Dunn

(f) Plasma Turbulence

Measurements of the plasma density and potential fluctuation will be made on the 3-meter plasma column device that is now almost completed. The necessary conditions for achieving weak or strong turbulence will be explored; parameters to be varied include magnetic-field gradient, neutral-particle density, plasma density and density gradient, and radial electric fields. Theoretical predictions of Kadomtsev, Taylor, and others will be tested when applicable.

D. J. Rose, J. C. Woo

(g) Interaction of Coherent Radiation and Plasmas

Work on laser-plasma interactions continues, based on the following accomplishments.

(i) Unambiguous large-angle Thomson scattering signals have been observed, and a study of the electron distribution function in the hollow-cathode discharge is being performed with the use of this technique.

(ii) Theoretical work on the photoionization of excited neutral atoms in a plasma by ruby laser radiation has led to a better understanding of the processes involved, as well as raising some interesting questions. An experiment has been constructed which we hope will lead to a successful resolution of these matters.

(iii) An experiment has been designed in which it is hoped to observe the transverse Doppler shift from relativistic electrons in a 5-kev beam. A valuable by-product of the experiment is the development of light-dumping techniques in order to detect the extremely small signal.

(iv) In view of the relatively large divergence of our ruby laser, we do not expect to investigate small-angle scattering from our plasmas at this wavelength. We intend, however, to capitalize on the high power output and low divergence of the argon laser in order to observe plasma correlation effects.

E. T. Gerry, E. Thompson

(h) Minimum B Confinement Systems

Minimum B confinement schemes offer interesting possibilities for stable plasma confinement. We are building a facility to test the confinement properties of one member of this family (the stuffed cusp) for hot electron plasmas. The plasma will be generated by beam-plasma interaction or by cyclotron resonance heating.

L. M. Lidsky, C. E. Wagner

(i) Nonadiabatic Motion of Charged Particles

We have extended our research on nonadiabatic injection schemes to include a more general study of charged-particle behavior under the action of weak nonadiabatic forces. Recent experiments have verified the results of first-order analyses of injection devices, and we are now investigating the higher order drift and diffusion rates. The principal experimental attack will be a study of the lifetime of electrons circulating in perturbed toroidal fields and in mirror systems.

L. M. Lidsky, J. F. Clarke, R. W. Moir

(j) Cesium Plasmas and Adsorption Systems

Properties of low-energy cesium plasmas are being investigated. We have calculated cross sections for the electron excitation of cesium atoms to the first excited state and for cesium molecular ion formation by collisions of two excited cesium atoms. A variety of transport effects are, at present, under study.

The chemical approach to intermetallic adsorption systems is now being extended to gases adsorbed on metals. Our objective is to predict theoretically such properties as electron work functions, and atom and ion desorption energies and rates for metallic surfaces covered by gases.

E. P. Gyftopoulos

A. BEAM-PLASMA DISCHARGE: SYSTEM A

We are continuing the experiments to measure the microwave radiation from a beam-plasma discharge.[1] The plasma is produced by an electron beam of up to 10 kv and 1 amp, which can be pulsed 30 pps and have a pulse length of 500 μsec. The plasma is contained by two Helmholtz coils that can produce 700 gauss at the center with a mirror ratio of

three. The drift region is 40 cm long. The vacuum has a base pressure of 2×10^{-6} torr.

The radiation is received by a microwave horn, detected by a Singer Panoramic SPA-4 spectrum analyzer, and the synchroscope output of the spectrum analyzer is observed on an oscilloscope. We have found that within certain frequency ranges, after an initial build-up period whose duration varies with pressure, the radiofrequency persists until the end of the beam pulse. It is quite "spikey" during this period, however. For low magnetic fields ($B < 120$ gauss) and relatively high pressures ($p > 3\mu$), this "long time" radiofrequency in hydrogen is linearly dependent on magnetic field. If radiation at the electron plasma frequency and an electron temperature of 150 ev is

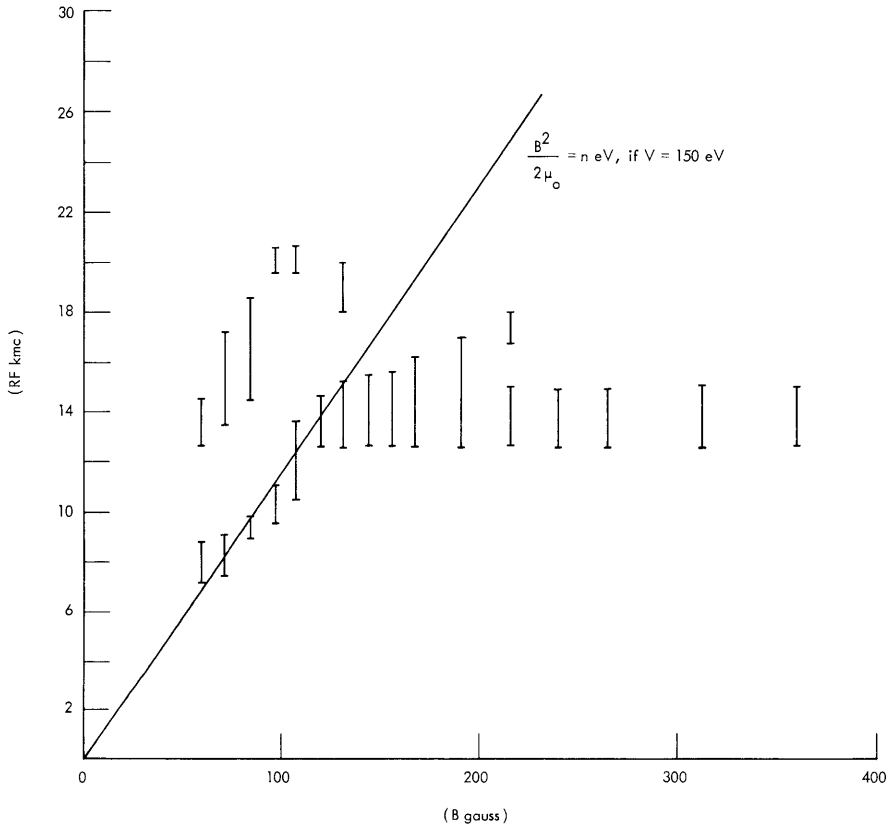

Fig. XV-1. Microwave radiation vs magnetic field. Pressure, 5.7 μ; beam voltage, 7 kv; beam current 0.55 amp; gas, H_2. Of the two bands that appear below 150 gauss, the lower is ~30 db stronger.

assumed,[2] then the density builds up until the kinetic pressure equals the magnetic pressure (Fig. XV-1). Above 120 gauss, however, the frequency of the emitted radiation appears to be independent of the magnetic field, and the band levels off around 14 kmc, thereby indicating a density of $n = 2.4 \times 10^{12}$ cm^{-3}. This limiting frequency increases

slowly with pressure, being approximately 14 kmc at 1.4 μ, and 16 kmc at 14 μ. The amplitude of the radiofrequency is a strong function of pressure, increasing 20 db from 1.4 μ to 5.7 μ, and increasing another 10 db from 5.7 μ to 14 μ.

For the conditions in Fig. XV-1, the light intensity increases with magnetic field up to 120 gauss, and then levels off along with the radiofrequency.

J. A. Davis

References

1. H. Y. Hsieh, Experimental Study of Beam-Plasma Discharge, Ph.D. Thesis, Department of Electrical Engineering, M.I.T., September 1964.

2. Ibid., p. 73.

B. BEAM-PLASMA DISCHARGE: SYSTEM C

In this report we discuss the interpretation of the magnetic probe used in System C. Figure XV-2 shows the problem to be analyzed. The plasma is created at t = 0 and the resulting diamagnetism is detected by a 22-turn coil wrapped around the outside of the stainless-steel drift tube, at z = 0. The interpretation of the coil voltage is made difficult by the time-dependent diffusion of the expelled flux through the stainless-steel drift tube, and the unknown plasma geometry.

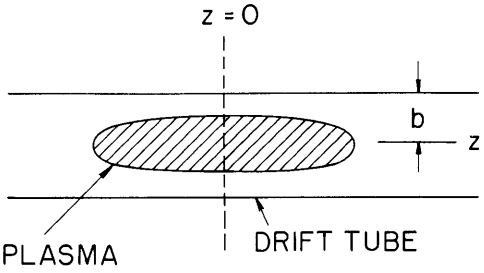

Fig. XV-2. Illustrating the problem.

The model used for the plasma is that of a low-β plasma whose magnetization $\vec{M}$ is uniform within a cylinder of radius a and length ℓ and zero elsewhere. To simplify the analysis we assume that (i) the displacement current can be neglected for the frequencies of interest, and (ii) the induced electric field is constant over the thickness of the drift tube. Assumption (ii) places an upper limit on the frequencies for which the result will be valid, namely, the frequency at which the skin depth is equal to the thickness of the tube.

With these assumptions, a boundary-value problem can be set up involving the vector potential $\vec{A}$. The equation to be solved is

$$\nabla^2\vec{A} = \begin{cases} \vec{i}_\phi \mu_o \dfrac{nw_\perp}{B}\delta(r-a) & |z| < \dfrac{\ell}{2} \\ 0 & |z| > \dfrac{\ell}{2} \end{cases} \qquad (1)$$

where $nw_\perp$ is the transverse energy density of the plasma, and A is subject to the boundary conditions

$$A_\phi\Big|_{r = b^+} = A_\phi\Big|_{r = b^-} \tag{2}$$

and

$$\frac{\partial A_\phi}{\partial r}\Big|_{r = b^+} - \frac{\partial A_\phi}{\partial r}\Big|_{r = b^-} = \mu_o \sigma \delta s A_\phi\Big|_{r = b} \tag{3}$$

where σ is the drift-tube conductivity, δ is the tube thickness, s is the Laplace transform variable, and $b^\pm$ are the outer and inner radii of the tube. Boundary condition (2) follows from the assumption of constant electric field, while boundary condition (3) equates the difference in magnetic fields to the total current flowing in the drift tube.

The problem can be solved by Fourier-transforming in the z coordinate and solving the resultant Bessel equation in the r coordinate so that the δ-function is obtained in (1). If homogeneous solutions to (1) are assumed for $r < b$ and $r > b$ and boundary conditions are applied, the potential can be found and evaluated to yield the total flux threading the coil at $z = 0$.

$$\Phi = 2\pi b A(r = b) = 4\mu_o ab \int_0^\infty du \frac{\sin u}{u} \frac{I_1\left(u\frac{2a}{\ell}\right)}{I_1\left(u\frac{2b}{\ell}\right)} \frac{\alpha}{s + \frac{\alpha}{K_1\left(u\frac{2b}{\ell}\right) I_1\left(u\frac{2b}{\ell}\right)}} \frac{nw_\perp}{B_o}. \tag{4}$$

where $\alpha = (\mu_o \sigma \delta b)^{-1}$.

For System C, $a, b \ll \ell$ and examination of the integrand in (4) reveals that small-argument expansions of the Bessel functions are in order. The integration can then be performed trivially to yield

$$\Phi \approx \mu_o \pi a^2 \left\{\frac{2\alpha}{s + 2\alpha}\right\} \frac{nw_\perp}{B_o}$$

which produces the coil voltage

$$E_c = sN\Phi \approx \mu_o \pi a^2 N \left\{\frac{2\alpha s}{s + 2\alpha}\right\} \frac{nw_\perp}{B_o}. \tag{5}$$

The time constant $(2\alpha)^{-1}$ in Eq. 5 is simply the L/R of the drift tube.

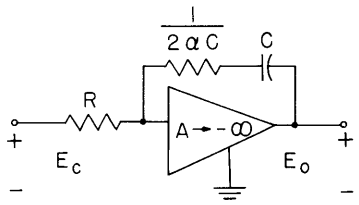

Fig. XV-3. Network realizing the system function.

The form of Eq. 5 suggests passing the coil voltage through a filter whose system function is proportional to $(s+2\alpha)/2\alpha s$. A network realizing this system function is shown in Fig. XV-3. The instantaneous transverse energy density is then related to the output of the filter by

$$nw = \frac{RCB_o}{\mu_o \pi a^2 N} e_o(t).$$

Numerically, the proportionality constant is approximately $10^{15}\ \frac{ev}{cc}/v$.

L. D. Smullin, W. D. Getty, R. R. Parker

C. BEAM PLASMA DISCHARGE: SYSTEM D

System D has been under construction for a year and has just been put into operation. It differs from System C in two important respects: the magnetic field is considerably stronger, and the drift tube diameter and length are greater. The magnetic field is provided by a system of coils designed to produce a mirror field with $B_{max} \approx 20,000$ gauss and $B_o \leq 10,000$ gauss. In order to provide the necessary DC power (~1 Mw, max), the system has been installed in Cell 2 of the National Magnet Laboratory. The drift tube is an aluminum cylinder 12 inches O.D. $\times \frac{1}{4}$ inch wall $\times$ 8 ft long. It is evacuated by a 10-inch oil diffusion pump, and liquid N_2 baffle. Figure XV-4 is a photograph of the system. [One of the four large coils is missing. It failed during preliminary testing and is being repaired. Thus, the system now under test uses only two of the large coils and all four of the smaller ones.]

The same magnetron-type, hollow-beam, electron gun is used as in System C, ~10 kv-10 amps, but the pulser has only a 300 μsec delay line as compared with 600 μsec in System C. (An additional 300-μsec section is under construction.)

Gas (H_2) is allowed to flow into the system continuously through the chamber over the pump, with the high-vacuum valve throttled to $\sim \frac{1}{3} - \frac{1}{4}$ opening. Under these conditions the base pressure is $3\text{-}4 \times 10^{-7}$ torr, and operating pressures have been in the range $10^{-5}\text{-}10^{-4}$ torr of hydrogen.

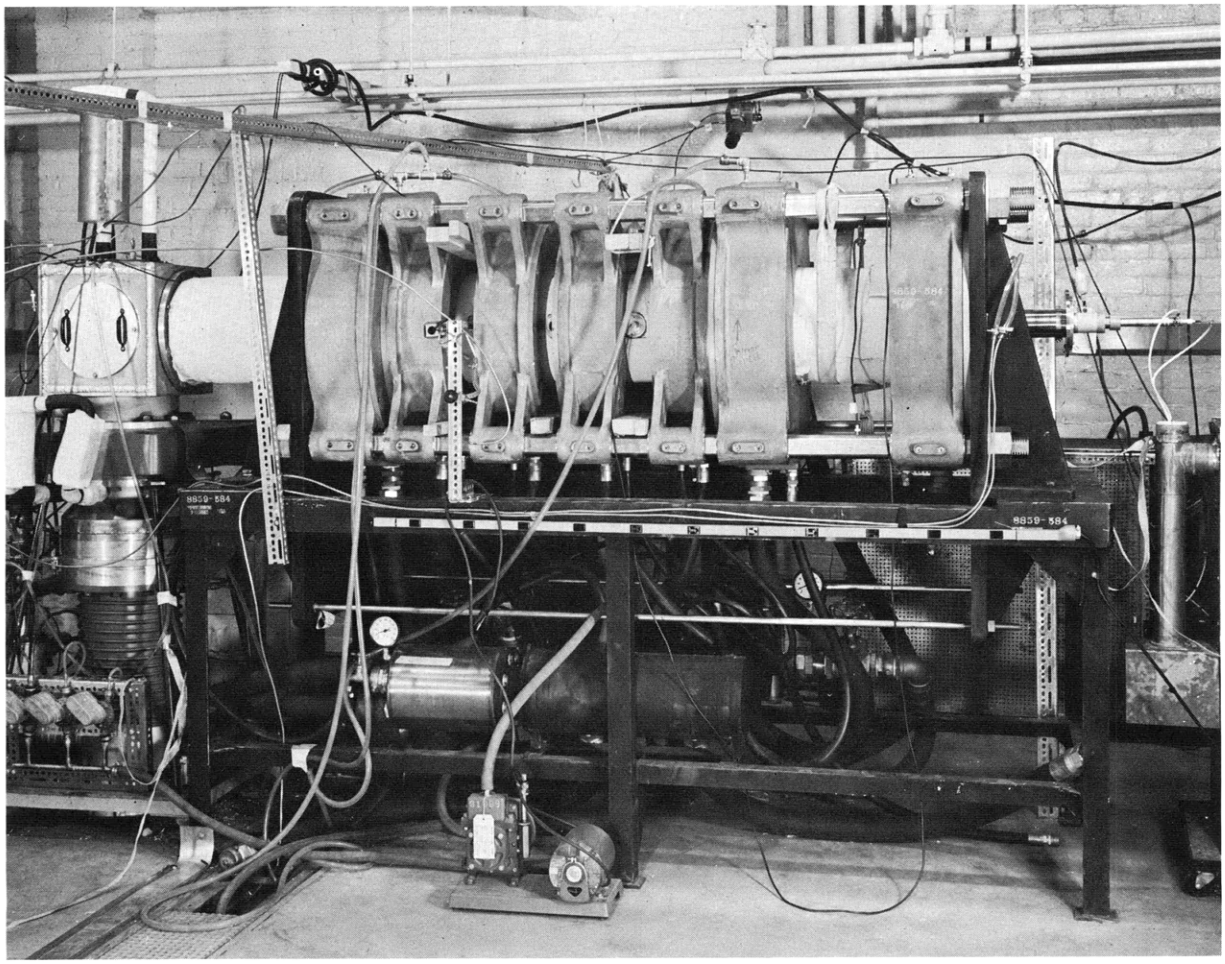

Fig. XV-4. System D.

1. Test Results

(a) The first tests were made with the magnets connected as shown in Fig. XV-5a, which results in the axial field strength indicated in Fig. XV-5b. The mirror ratio was ~2, and the plasma generated by the 10 kv-10 amp beam was very "weak" at all pressures up to $\sim 10^{-3}$ torr. The light was much less intense than in System C, and there were no detectable x-rays.

(b) In the next series of tests, the magnets were connected as shown in Fig. XV-6a, to produce a mirror ratio of 3:1 (Fig. XV-3b). The results were dramatically different, and the resultant plasma produced strong visible and x radiation and a large diamagnetic signal. There appeared to be a new type of gun breakdown in which the low resistance path was from gun to collector (~4 ft). The breakdown usually occurs during the last 50-100 μsec of the beam pulse, and is characterized by a sudden increase in both cathode and collector currents. It is believed that this is caused by the plasma column

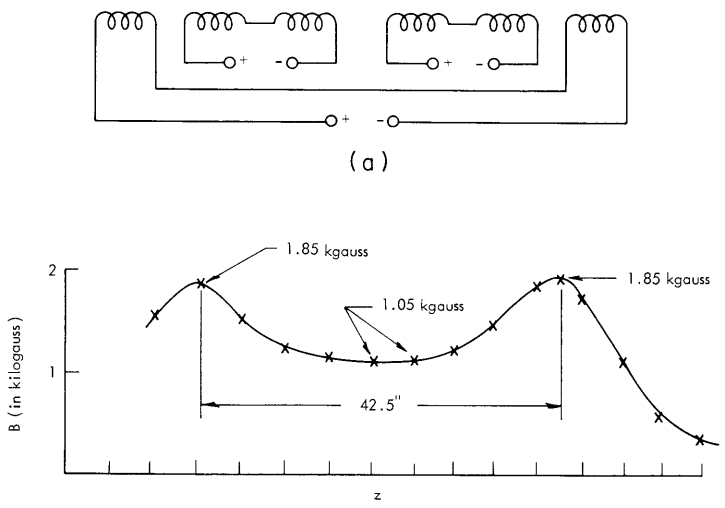

Fig. XV-5. Axial field strength of magnet system with coil connections indicated (I_{total} = 1000 amps).

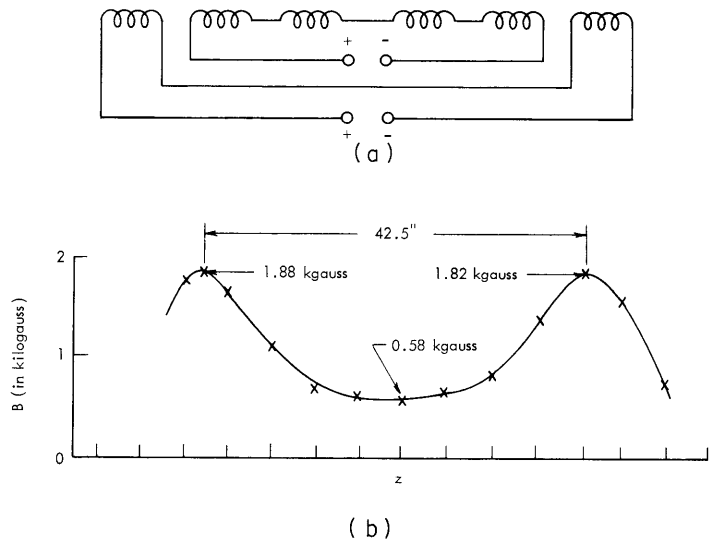

Fig. XV-6. Axial field strength of magnet system with coil connections indicated (I_{total} = 1000 amps).

reaching through the mirror and shorting the cathode and anode together. A first attempt to correct this embodied a restriction over the anode. It appeared to be partly successful, and operation was possible at voltages up to 13-14 kv.

The diamagnetic expulsion of field by the plasma was measured by a 20-turn coil wound on an aluminum ring that had an insulating break in it. The coil was placed inside

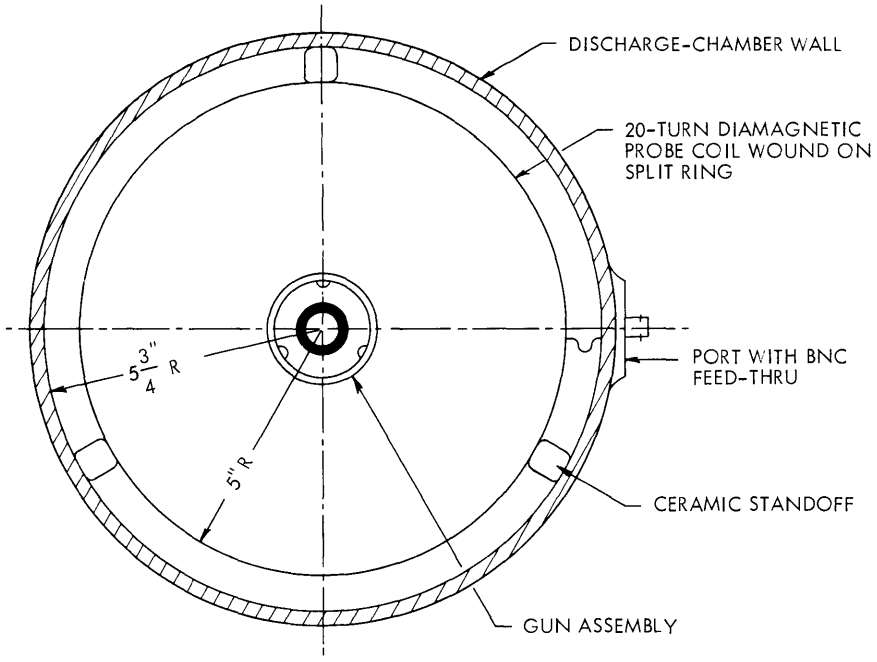

Fig. XV-7. Diamagnetic probe – axial view from collector end.

the drift tube (see Fig. XV-7). For times short compared with the L/R time constant of the 1/4 inch thick aluminum wall, 20 msec, the flux expelled from the plasma column piles up against the wall, thus momentarily increasing the external magnetic pressure on the plasma column.

There has been little time to take systematic data on the beam-plasma discharge in System D. The x-rays show a relatively smooth decay that can last for almost 1 second. The light appears to take 1-5 msec to decay after the beam pulse. (In System C the corresponding time is 100-300 μsec.)

L. D. Smullin, T. Musha, R. R. Bartsch

D. INTERACTION OF AN ELECTRON BEAM WITH A HOT-ELECTRON PLASMA

We have previously reported an experiment in which an electron beam was modulated at low frequencies (10-200 Mc) and injected into a hot-electron plasma created by an electron-cyclotron resonance discharge (ECRD).[1,2] We observed a pronounced enhancement of the beam modulation when the hot-electron plasma was present, an enhancement which was peaked at around 60 Mc.[3] To study this beam-plasma interaction more carefully, the experiment has been shifted to a new apparatus and provided with a more powerful source of microwave energy. The principal advantage of the shift is an increase in the interaction distance from 8 inches to more than 2 feet. The microwave power level has been increased tenfold to 1000 watts.

In order to construct a theoretical model of this experiment, it is desirable to know the zero-order, unperturbed properties of both the electron beam and the plasma that the ECRD generates. We can easily measure the "diameter" of the beam and determine the beam density and beam velocity from a knowledge of the beam current and voltage. On the other hand, the properties of the plasma are not so easily determined. Thus we decided to concentrate initially on diagnostics designed to measure the properties of the ECRD plasma in the absence of the beam.

We are now in the process of assembling and testing a microwave interfermoeter to measure the electron density of the plasma. We use a resonating, or Fabry-Perot, interferometer, rather than a conventional Michelson type. The extremely sharp fringes of a resonating interferometer allow the measurement of very small phase shifts. This in turn permits the use of an interferometer working frequency that is relatively far above the plasma cutoff frequency. The plasma will thus perturb the microwave field configuration slightly. Furthermore, the use of a higher frequency and the focusing action of the microwave mirrors results in a very tightly focused beam of microwave power.

The interferometer is designed to operate at 8-mm wavelength. A phase shift of approximately 30° will be obtained when the electron density rises to 5×10^{10}/cc, corresponding to 100 per cent ionization of hydrogen gas at a pressure of 10^{-6} torr. The half-power diameter of the microwave beam will be approximately 3/4 inch.

A retarding potential probe has been assembled and mounted in the anode pole piece. This probe is designed to measure the energy distribution of the plasma electrons. It consists of a copper tube, 1 inch in diameter, containing three grids and a plate. The tube is covered with a copper cap containing a small hole to sample the plasma. When in use, the plate current is measured as a function of control grid voltage. Only those electrons reach the plate whose energies are high enough to climb the retarding potential of the control grid. Using this probe in the ECRD plasma with hydrogen gas, we have obtained several curves plotting plate current against grid voltage, but have not yet analyzed them.

We have observed integrated x-ray fluxes as great as 25 roentgens/hour when the ECRD is excited. This is a thousandfold increase in flux over the old apparatus, and provides evidence of hot electrons. We shall soon study the energy spectrum of these x-rays by measuring, as a function of thickness, their absorption in sheets of various materials.

The collector and electron-gun assemblies are ready to be mounted in the new apparatus. Duplication of the experiment performed in the old apparatus will then be attempted.

M. A. Lieberman, L. D. Smullin

References

1. M. T. Vlaardingerbroek, M. A. Lieberman, and L. D. Smullin, Beam-excited ion-plasma oscillations, Quarterly Progress Report No. 72, Research Laboratory of Electronics, M.I.T., January 15, 1964, p. 125.

2. M. T. Vlaardingerbroek and M. A. Lieberman, Beam-excited ion-plasma oscillations, Quarterly Progress Report No. 73, Research Laboratory of Electronics, M.I.T., April 15, 1964, p. 70.

3. M. A. Lieberman and M. T. Vlaardingerbroek, Ion plasma oscillations, Quarterly Progress Report No. 74, Research Laboratory of Electronics, M.I.T., July 15, 1964, p. 120.

E. FURTHER ANALYSIS OF INTERACTIONS OF AN ELECTRON BEAM WITH IONS IN A WARM PLASMA

Previous reports have treated the azimuthally independent interactions between an electron beam and a warm plasma in systems of finite transverse geometry.[1-3] In this report we show that similar results are obtained in unbounded systems when waves of complex wave vector propagating at an angle with respect to the static magnetic field are considered. Recently developed stability criteria[4] are used to determine the nature of waves in the system. A physical interpretation of nonconvective instabilities in the system is given through consideration of the small-signal power flow associated with each wave.

1. Analysis of the Dispersion Equation

The system analyzed here consists of a homogeneous plasma and electron beam, both of infinite extent. A uniform static magnetic field is applied in the z direction, parallel to the electron drift. The beam and plasma are described by collision-free, nonrelativistic transport theory. Thermal motions of beam electrons and plasma ions are ignored. In the longitudinal wave approximation,[5] the dispersion equation becomes

$$\bar{k} \cdot \bar{\bar{K}} \cdot \bar{k} = 0, \tag{1}$$

where waves having space-time dependence $\exp[j(\omega t - \bar{k} \cdot \bar{r})]$ are assumed.

A large magnetic field for which the conditions

$$\left|\frac{\bar{k}v_{Te}}{\omega_{ce}}\right| \ll 1 \tag{2}$$

and

$$\omega_{ce} \gg \omega,\ \omega_{pi},\ \omega_{ci},\ \omega_{pe},\ \omega_{pb} \tag{3}$$

are satisfied is assumed. With a wave vector of the form $k_\perp \bar{i}_x + k_{||} \bar{i}_z$, the dispersion equation becomes

$$k_{||}^2\left[1 - \frac{\omega_{pi}^2}{\omega^2} - \frac{\omega_{pe}^2}{\omega^2 - k_{||}^2 v_{Te}^2} - \frac{\omega_{pb}^2}{(\omega - k_{||}v_o)^2}\right] = -k_\perp^2\left[1 - \frac{\omega_{pi}^2}{\omega^2 - \omega_{ci}^2}\right]. \tag{4}$$

If $k_\perp$ is arbitrarily restricted to a fixed real value, this dispersion equation is identical to that found for the waveguide system previously analyzed.[1-3] We assume in the sequel that $k_\perp$ has been so chosen. The unbounded system then has essentially the same properties as the waveguide system, but it is not necessary to consider the possible effects of conducting boundaries close to the region of interest.

It is worth while to notice how the dispersion equation may be scaled to different values of electron temperature and beam voltage. For the scaling to be considered, the ratio v_{Te}/v_0 or T_e/V_0, the magnetic field, and the number densities of the various particle species present are held constant. When v_{Te} and v_0 are replaced by v_{Te}/a and v_0/a, where a is a positive real number, the same dispersion equation is recovered if $\bar{k}$ is replaced by $a\bar{k}$. This indicates that instabilities previously analyzed[1] occur at smaller absolute values of electron temperature and beam voltage, provided the wavelength of the disturbance is made correspondingly shorter, within the limitations of Eq. 2. A further implication of this particular form of scaling is that spatial growth rates of convective instabilities become larger for smaller absolute values of v_{Te} and v_0.

a. "Low-Temperature" Domain, $\frac{T_e}{V_0} < 1$

When the electron temperature is less than the beam voltage, the system supports a convective instability. The mechanism for this instability appears to be reactive medium

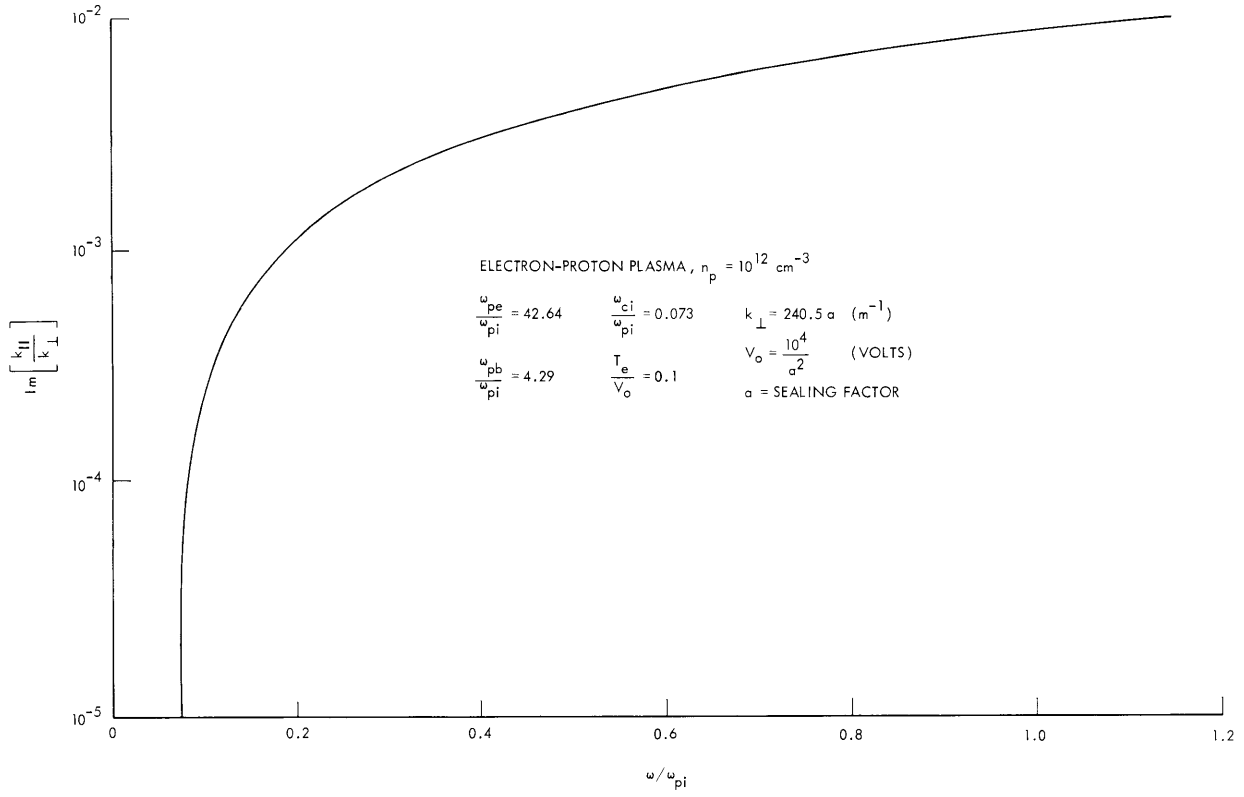

Fig. XV-8. Spatial growth rate of the convective instability, $\frac{T_e}{V_0} < 1$.

amplification. This instability is present at frequencies from ω_{ci} to above ω_{pi}. The spatial growth rate varies slowly with frequency and is relatively insensitive to changes in electron temperature. Figure XV-8 shows a plot of the calculated growth rate versus frequency for one particular case.

b. "High-Temperature" Domain, $\frac{T_e}{V_0} > 1$

When the electron temperature is greater than the beam voltage, either a convective or a nonconvective instability may be present, as has been reported previously.[1] The convective instability, which has a spatial growth rate strongly dependent on electron temperature, exists for frequencies from ω_{ci} to ~0.5 ω_{pi}. Transition from the convective to the nonconvective mode of instability is controlled by both the beam density and the electron temperature.

Figure XV-9 shows the calculated growth rate of the convective instability as a function of frequency for one particular case. Figure XV-10 shows the conditions for which transition from the convective to the nonconvective instability occurs. For these calculations, the ratio T_e/V_0 has been emphasized, rather than the absolute values of T_e

and V_0. Also, plasma electron density has been varied to maintain over-all space-charge neutrality with changes in beam density. This last detail was overlooked in previous work.[1]

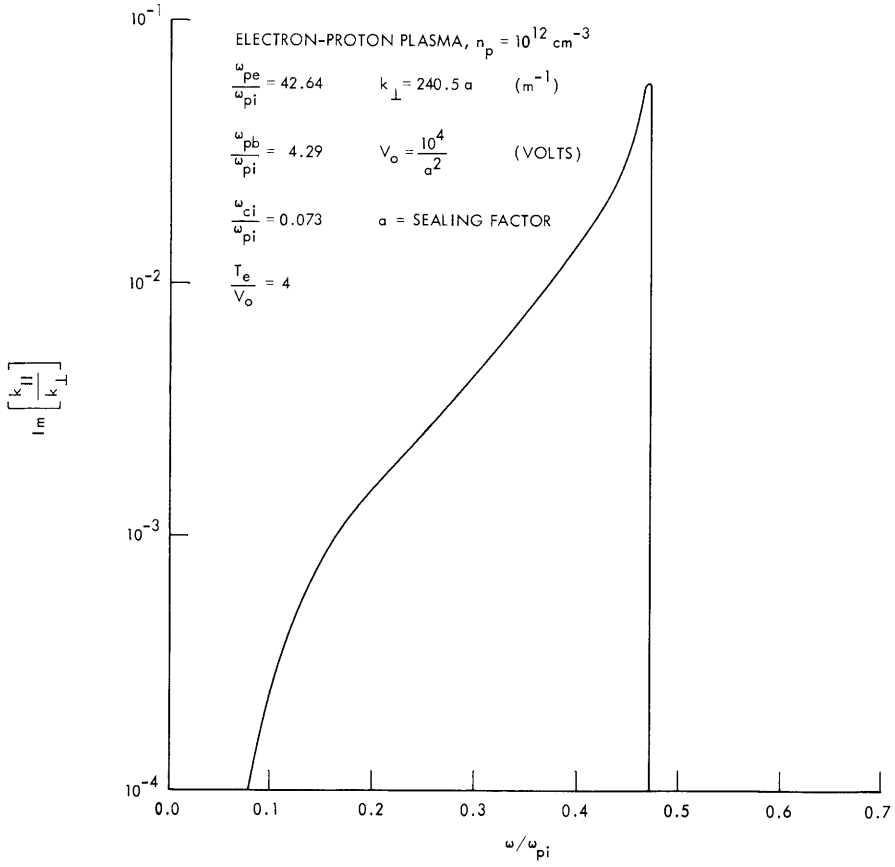

Fig. XV-9. Spatial growth rate of the convective instability, $\frac{T_e}{V_0} > 1$.

2. Small-Signal Power Flow in Complex Waves

By combining the results of previous analyses,[6,7] the time-averaged power flow per unit area in the direction of the magnetic field can be found for the longitudinal wave approximation. This power takes the form

$$\langle P_z \rangle = \frac{1}{2} \text{Re} \left\{ \phi J_{tz}^* + U J_{bz}^* + \frac{m_e v_{Te}^2}{n_{oe}} n_{1e} \Gamma_{ez}^* \right\}. \tag{5}$$

The subscripts 0 and 1 denote zero- and first-order quantities, respectively. The unfamiliar terms in this equation are defined as follows:

$\phi = \Phi \exp[j(\omega t - \bar{k}\cdot\bar{r})]$, scalar electric potential

$U = \dfrac{v_0 v_{1b}}{\frac{e}{m_e}}$, kinetic voltage of the electron beam

J_b = first-order beam current

$\bar{\Gamma}_e$ = plasma electron particle flux

There is no time-averaged power flow in the direction transverse to the magnetic field, provided $k_\perp$ is taken real and perfectly conducting boundary planes at $x = \pm\infty$ are assumed. This is equivalent to considering "elementary" wave solutions composed of the sum of two single-wave solutions having equal amplitudes and equal values of $k_{||}$, but with $k_\perp$ of opposite sign.

In order that energy be conserved in the system, wave solutions must satisfy the condition $\dfrac{\partial \langle P_z \rangle}{\partial z} = 0$. For single waves, this implies that $\langle P_z \rangle$ vanishes unless k is real. Pairs of waves, denoted by subscripts c and d, having $k_{||}$ complex may carry finite power if $k_{||c} = k^*_{||d}$. The power per unit area consists of cross terms between the two waves:

$$\langle P_{z\text{-cross}} \rangle = \frac{1}{2} \mathrm{Re} \left\{ \phi_c J^*_{tzd} + \phi_d J^*_{tzc} + U_c J^*_{bzd} + U_d J^*_{bzc} + \frac{m_e v^2_{Te}}{n_{1e}} \left(n_{1ec} \Gamma^*_{ezd} + n_{1ed} \Gamma^*_{ezc} \right) \right\} \tag{6}$$

To gain some insight into the nature of the nonconvective instability which the system supports, the individual terms in the expression for $\langle P_z \rangle$ were evaluated. Writing $\langle P_z \rangle$ entirely in terms of the electric potential gives

$$\langle P_z \rangle = \mathrm{Re} \left\{ -\frac{1}{2} \omega k^*_{||} \left[1 - \frac{\omega^2_{pi}}{\omega^2} - \frac{\omega^2_{pe}}{\omega^2 - k^{*2}_{||} v^2_{Te}} - \frac{\omega^2_{pb}}{(\omega - k^*_{||} v_0)^2} \right] + \frac{1}{2} \frac{\omega^2_{pb} \omega v_0 |k_{||}|^2}{(\omega - k_{||} v_0)(\omega - k^*_{||} v_0)^2} + \frac{1}{2} \frac{\omega^2_{pe} v^2_{Te} \omega k_{||} |k_{||}|^2}{|\omega^2 - k^2_{||} v^2_{Te}|^2} \right\} \epsilon_o |\phi|^2. \tag{7}$$

The three main terms in this expression are the electromagnetic, kinetic, and acoustic power flows associated with the wave under consideration.

From the stability criteria,[4] the two waves that join to form the absolute instability and the direction of signal propagation associated with each wave are known. Assuming,

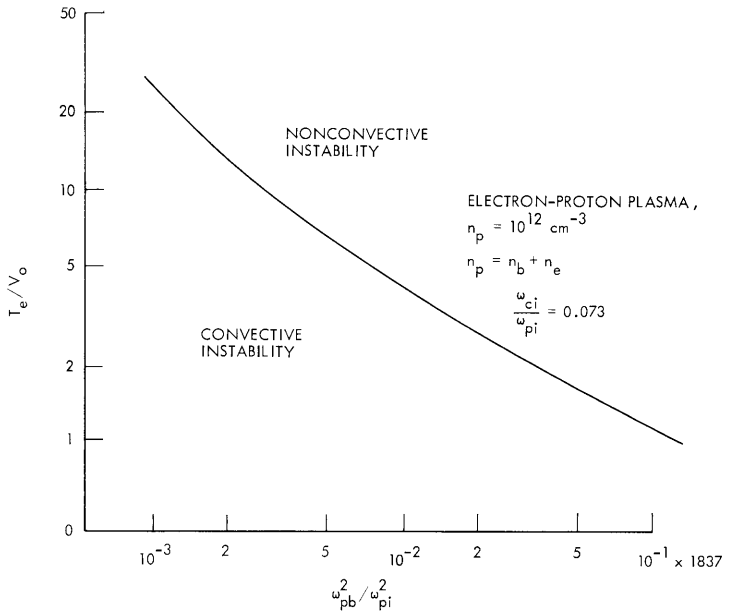

Fig. XV-10. Transition from convective to nonconvective instability.

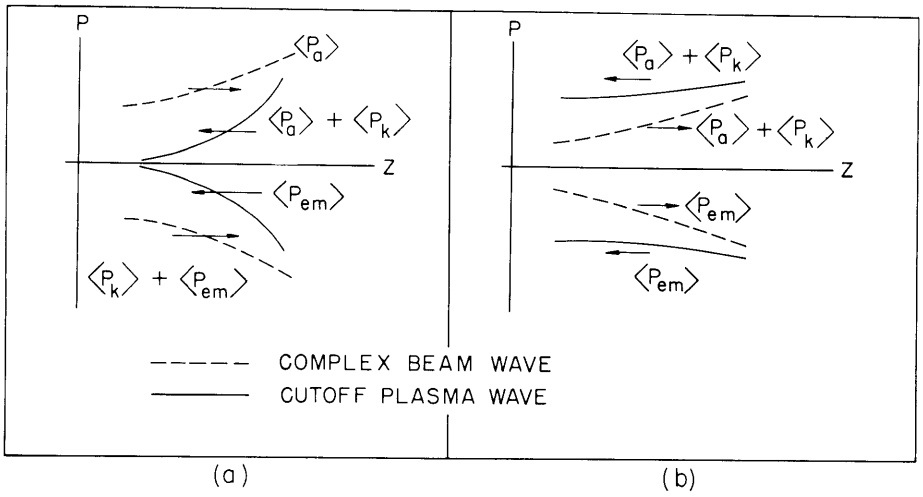

Fig. XV-11. Qualitative description of power flows leading to the nonconvective instability. (a) With convective instability. (b) With nonconvective instability. (Arrows denote direction of signal travel.)

for a given set of system parameters, that ϕ is the same for the two waves, one can compare the power flows associated with each. This comparison is shown in Fig. XV-11. A real frequency approximately equal to that for which the nonconvective instability first appears was chosen. When the system parameters are such that only the convective instability is present, the power level in the "cutoff plasma wave" is smaller than that of the "complex beam wave" and the decay rate of the former wave toward negative z exceeds the growth rate of the latter toward positive z. For system parameters that produce the nonconvective instability but lead to growth rates in time sufficiently small that time averages can still be defined, the power level of the "cutoff plasma wave" exceeds that of the "complex beam wave." The growth rate of the latter toward positive z exceeds the decay rate of the former toward negative z. The net power in each wave alone vanishes as required for conservation of energy.

If coupling between these two waves is assumed, then it is apparent that, with the convective instability, disturbances carried toward positive z by the "complex beam wave" would be returned by the "cutoff plasma wave" with smaller amplitude. The "loop gain" of the system is less than unity, and no self-sustaining oscillations are produced. When the nonconvective instability is present, the "loop gain" of the system is greater than unity and growing oscillations are produced. Thus, coupling between the "complex beam wave" and the "cutoff plasma wave" apparently provides the internal feedback necessary to cause the nonconvective instability.

A thesis concerning this work was submitted by R. N. Wallace to the Department of Electrical Engineering, M.I.T., September 2, 1964, in partial fulfillment of the requirements for the degree of Master of Science.

R. N. Wallace, A. Bers

References

1. A. Bers, S. Puri, and J. D. Mills, Quarterly Progress Report No. 74, Research Laboratory of Electronics, M.I.T., July 15, 1964, pp. 121-128.

2. R. J. Briggs and A. Bers, Quarterly Progress Report No. 71, Research Laboratory of Electronics, M.I.T., October 15, 1963, pp. 131-137.

3. R. J. Briggs and A. Bers, Quarterly Progress Report No. 70, Research Laboratory of Electronics, M.I.T., July 15, 1963, pp. 129-133.

4. A. Bers and R. J. Briggs, Quarterly Progress Report No. 71, Research Laboratory of Electronics, M.I.T., October 15, 1963, pp. 122-131.

5. T. H. Stix, The Theory of Plasma Waves (McGraw-Hill Book Company, Inc., New York, 1962).

6. R. J. Briggs, On the Quasistatic Analysis of Guided Waves in Plasmas and Electron Beams, Internal Memorandum, Research Laboratory of Electronics, M.I.T., October 17, 1962.

7. W. P. Allis, S. J. Buchsbaum, and A. Bers, Waves in Anisotropic Plasmas (The M.I.T. Press, Cambridge, Mass., 1963.

F. INSTABILITIES IN PLASMAS WITH BEAMS INJECTED ACROSS THE MAGNETIC FIELD

We have studied some of the instabilities that may arise in systems consisting of a beam of charged particles of finite dimensions (thickness τ) injected with velocity v_0 into a plasma across the confining magnetic field, B_0. ($v_0 \perp B_0$.) We report our results for two limiting cases of interest. (i) Beam thickness large compared with the wavelength along v_0; these we call body-type, or internal, instabilities. (ii) Beam thickness small compared with the wavelength along v_0; these we call surface-type instabilities. In the analysis for all cases the quasi-static approximation is used.

1. Body-type Instabilities ($k_\perp \tau \gg 1$).

This case is illustrated in Fig. XV-12. Our interest here is only in short-wavelength perturbations either along v_0, ($k_\perp \| v_0$), or B_0, ($k_\| \| B_0$). We assume uniformity is the

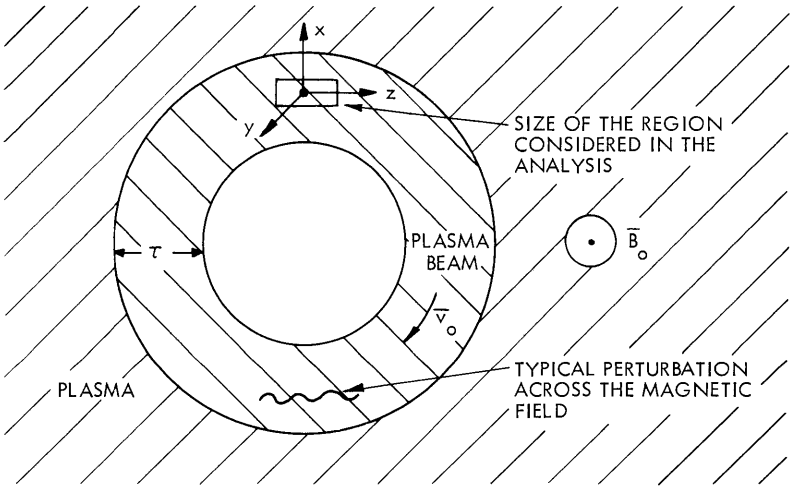

Fig. XV-12. Thick-beam model: Beam flowing through a plasma across the magnetic field.

direction perpendicular to both v_0 and B_0, neglect the effect that is due to the finite curvature of the beam, and fix $k_\perp v_0 = n\omega_{cb}$, where ω_{cb} is the cyclotron frequency for the beam particles, and n is an integer. Two distinct types of instabilities are found.

a. $k_\| \gg k_\perp$: Short-Wavelength Perturbations along B_0

For a cold beam and cold plasma these are of the type first discussed by Burt and Harris.[1] The dispersion relation is

$$\frac{\omega_{pb}^2}{(\omega - n\omega_{cb})^2} \cong K_{\parallel p}$$

$$= 1 - \frac{\omega_{pp}^2}{\omega^2}, \tag{1}$$

where ω_{pb} and ω_{pp} are the plasma frequencies for the beam particles and plasma particles, respectively. The condition for instability follows from Eq. 1, and is

$$\left[1 + \frac{\omega_{pb}^{2/3}}{\omega_{pp}^{2/3}}\right]^{3/2} \omega_{pp} > n\omega_{cb} \tag{2}$$

as can also be seen from a graphical solution of Eq. 1, shown in Fig. XV-13. For an ion beam of low density, instability set in when roughly $\omega_{pp} > \omega_{ci}$, as found by Burt and

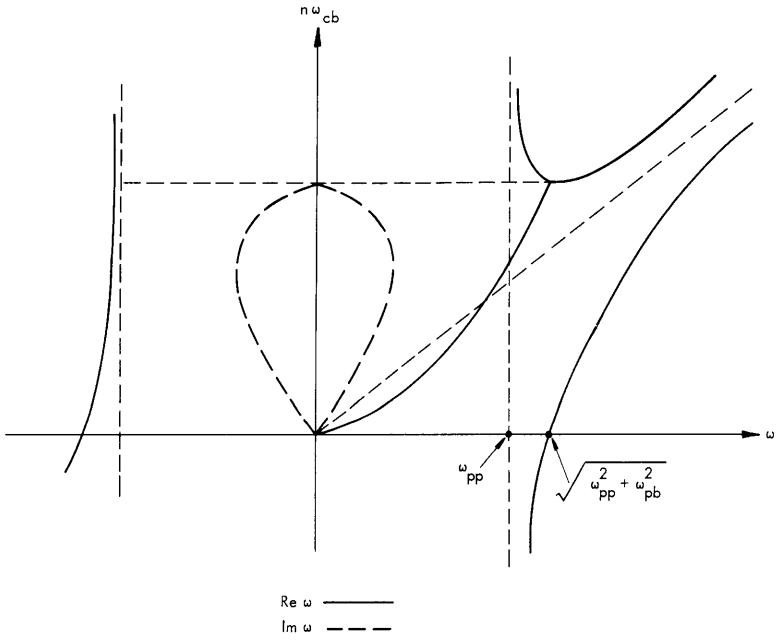

Fig. XV-13. Solution of Eq. 1.

Harris. For an electron beam of low density, instability sets in when $\omega_{pp} > \omega_{ce}$. As an example consider $\left(\omega_{pb}^2/\omega_{pp}^2\right) = 0.1$, then the maximum growth rate is found at $\omega_r \approx \omega_{pp} \approx n\omega_{cb}$ and is $|\omega_{i\,max}| \approx 0.25\,\omega_{pp}$. We note that the maximum growth rate occurs for frequencies at which the plasma by itself would just be reactive ($K_{\parallel p} \gtrsim 0$). This

instability may then be classified as resulting from a longitudinal, reactive plasma-medium interaction.

The effects of finite temperature can be seen from the following simple model. Assume that the electrons of the plasma are characterized by a Maxwellian velocity distribution with $v_{Te} \ll v_0$. Also assume that the beam particles are injected with a velocity spread v_{Tb} about v_0. For low temperatures, under the assumption $k_\perp v_0 = n\omega_{cb}$, the dispersion relation, as before, is approximately

$$\frac{\omega_{pb}^2}{(\omega - n\omega_{cb})^2 - 3\left(n\omega_{cb}\frac{v_{Tb}}{v_o}\right)^2} \approx 1 - \frac{\omega_{pp}^2}{\omega^2}\left(1 + \frac{3k_\parallel^2 v_{Te}^2}{\omega^2}\right). \tag{3}$$

For stability near $\omega \sim \omega_{pp}$, we find from Eq. 3

$$\frac{v_{Tb}}{v_o} > \frac{1}{3}\frac{\omega_{pb}}{n\omega_{cb}}\frac{\omega_{pp}}{k_\parallel v_{Te}}. \tag{4}$$

Since the onset of the instability is for approximately $n\omega_{cb} = \omega_{pp}$ (Eq. 2), we note that stability can be assured for reasonable beam-velocity spreads, v_{Tb}, and plasma electron velocity spreads, v_{Te}, provided the beam density is not too high.

b. $k_\perp \gg k_\parallel$: Short-Wavelength Perturbations along v_o

For a cold beam and cold plasma the dispersion relation is

$$\frac{\omega_{pb}^2}{(\omega - n\omega_{cb})^2 - \omega_{cb}^2} \cong K_{\perp p}$$

$$= 1 - \frac{\omega_{pe}^2}{\omega^2 - \omega_{ce}^2} - \frac{\omega_{pi}^2}{\omega^2 - \omega_{ci}^2}. \tag{5}$$

A graphical solution of Eq. 5 shows that in general there are two regions of possible instabilities (Fig. XV-14). The maximum growth rates occur at approximately $K_{\perp p} \ll 0$, and the instability may be classified as resulting from a transverse, reactive plasma-medium interaction. The sufficient conditions for these instabilities are

$$\omega_{0h} < n\omega_{cb} \lesssim \omega_{x\ell} \tag{6}$$

$$\omega_{0h} < n\omega_{cb} \lesssim \omega_{xh}, \tag{7}$$

where $\omega_{x\ell}$ and ω_{xh} are the resonances of the extraordinary wave in the plasma ($K_{\perp p} = 0$),

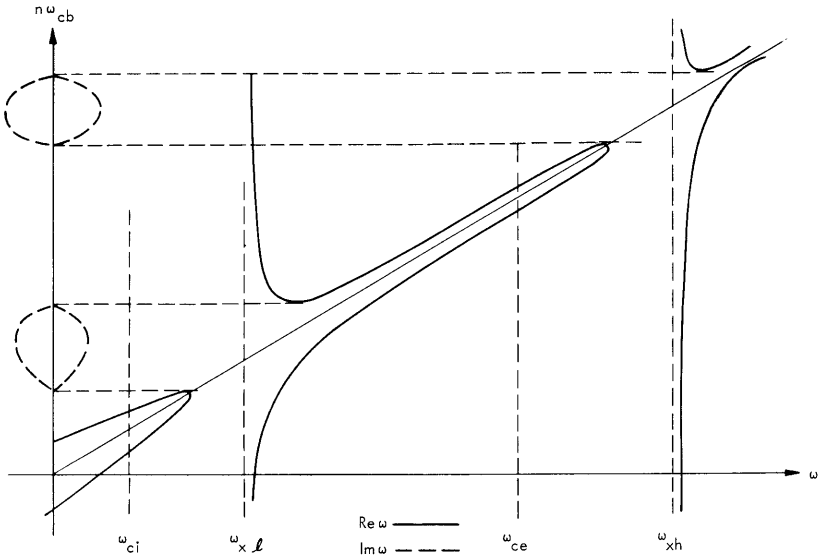

Fig. XV-14. Solution of Eq. 5.

and $\omega_{0\ell}$ and ω_{0h} are the frequencies for which $K_{\perp p} = -\omega_{pb}^2/\omega_{cb}^2$. For an electron beam and a low-density plasma for which Eq. 2 is not satisfied, Eqs. 6 and 7 show that instabilities may exist at the plasma electron cyclotron frequency. For a finite thermal velocity spread in the plasma electrons, resistive-type instabilities may arise at the electron cyclotron frequency and its harmonics.

2. Surface-type Instabilities ($k_\perp \tau \ll 1$).

This case is illustrated in Fig. XV-15. We again assume that the radius of curvature of the beam trajectory is large compared with the wavelength along the beam and that the system is uniform along B_0. We shall consider the case of a cold beam and cold plasma. The plasma is assumed to neutralize the beam. The over-all system is neutral and no DC electric fields are present. The method of solution for the thin beam was to find boundary conditions relating the fields just outside the beam to the fields just inside the beam, to write force equations in terms of the average fields within the beam, and to invoke the equations governing waves in a transversely magnetized, cold, collisionless plasma. These relations enabled us to find a determinantal equation. [The details may be found in the thesis of R. R. Bartsch.[2]]

The model of the thin beam in free space was the same as that used by Haus and Bobroff[3] (Fig. XV-15). The two motions of the beam are represented by two first-order surface charge densities on the beam: $\pm\sigma_{pol}$ at the upper and lower beam surfaces representing the snaking motion, and σ_1 the net first-order change per unit area representing the bulging motion. σ_1 and σ_{pol} are related to first-order velocities of the beam particles by

$$\sigma_1 = \frac{k_z \tau \rho_0}{\omega - k_z v_0} v_{1z} \tag{8}$$

$$\sigma_{pol} = \frac{\rho_0}{j(\omega - k_z v_0)} v_{1x} \tag{9}$$

where k_z is the propagation constant along the beam, ρ_0 is the beam charge density, τ is the beam thickness, v_0 is the DC beam velocity, and v_{1x} and v_{1z} are first-order

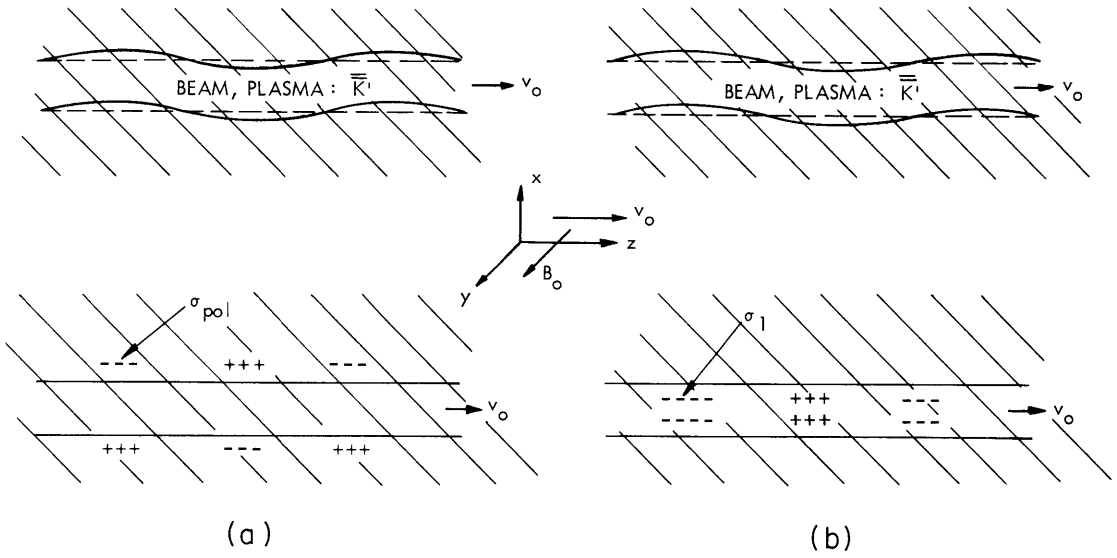

Fig. XV-15. Modes of thin beam in free space. (a) Snaking. (b) Bulging.

velocities. The force equations relating v_{1x} and v_{1z} to the average fields inside the beam are given by

$$v_{1x} = \frac{e/m}{\Omega^2 - \omega_c^2} (j\Omega \langle E_x \rangle + \omega_c \langle E_z \rangle) \tag{10}$$

$$v_{1z} = \frac{e/m}{\Omega^2 - \omega_c^2} (j\Omega \langle E_z \rangle - \omega_c \langle E_x \rangle), \tag{11}$$

where Ω is $\omega - k_z v_0$.

$$\langle E_x \rangle \equiv \frac{1}{2}(E_{x+} + E_{x-}) \tag{12}$$

and

$$\langle E_z \rangle \equiv \frac{1}{2}(E_{z+} + E_{z-}), \tag{13}$$

where + and - indicate transverse positions just inside the upper and lower beam boundaries, respectively. The fields just above and below the beam (denoted by subscripts a and b) and the fields inside the beam are related to the equivalent surface charges and to each other through the boundary conditions for the fields. These boundary conditions have been developed analogously with the usual boundary conditions for the case of a medium filled with cold collisionless plasma:

$$K_{\perp} E_{xa,b} + K_x E_{za,b} - K'_{\perp} E_{x+,-} - K'_x E_{z+,-} = \frac{\sigma_{pol}}{\epsilon_o} \tag{14}$$

$$E_{z+,-} = E_{za,b} \tag{15}$$

$$\bar{i}_x \cdot [\bar{\bar{K}} \cdot (\bar{E}_a - \bar{E}_b) - (\bar{\bar{I}} - \bar{\bar{K}}') \cdot (\bar{E}_+ - \bar{E}_-)] = \frac{\sigma_1}{\epsilon_0} \tag{16}$$

$$E_{za} - E_{zb} = \frac{jk_z \tau}{K'_{\perp}} \left(\frac{\sigma_{pol}}{\epsilon_0} + K'_x \langle E_z \rangle \right). \tag{17}$$

The primes denote dielectric tensor elements of the plasma inside the beam, and the meaning of the subscripts on the field terms is shown in Fig. XV-16.

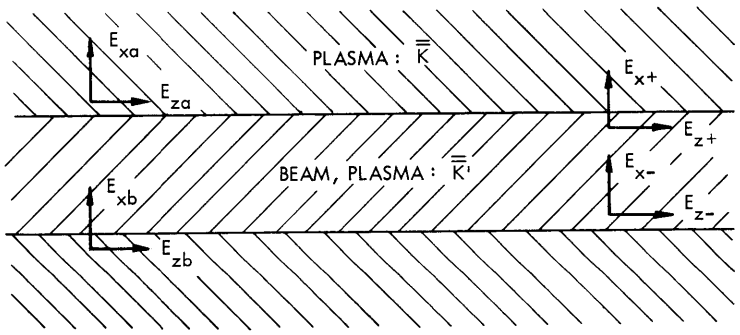

Fig. XV-16. Definitions of electric fields at beam edge.

The equations describing a transversely magnetized plasma[4] give us the two remaining relations necessary for solving for the dispersion relation of the system

$$E_{xa} = \frac{jk_z p - \frac{\omega^2}{c^2} K_x}{-k_z^2 + \frac{\omega^2}{c^2} K_{\perp}} E_{za} \tag{18}$$

$$E_{xb} = \frac{-jk_z p - \frac{\omega^2}{c^2} K_x}{-k_z^2 + \frac{\omega^2}{c^2} K_\perp} E_{zb}, \tag{19}$$

where

$$p^2 = k_z^2 - \frac{\omega^2}{c^2}\left(\frac{K_x^2 + K_\perp^2}{K_\perp}\right). \tag{20}$$

The dispersion equation resulting from the solution of Eqs. 8-20 has been analyzed for the case $\omega \approx k_z v_0$ with k_z real (equal to $2\pi n/R_c$, where "n" is an integer and R_c is the radius of curvature of the DC beam trajectory). The result is

$$\omega \approx k_z v_0 \pm \frac{\frac{\omega_{pb}^2}{\omega_c}\frac{v_0}{c} k_z \tau}{4\sqrt{K_\perp}}. \tag{21}$$

An instability of the reactive medium type is found approximately in the region $K_\perp \lesssim 0$. Since $K_\perp$ is a function of ω, the exact region must be found by solving Eq. 21 for ω and observing the ranges in which ω is complex.

The appropriateness of the thin-beam model is still being investigated. Questions about the motion of the beam particles and the motion of the internal plasma electrons at the beam surface have not been resolved.

A. Bers, R. R. Bartsch

References

1. P. Burt and E. G. Harris, Unstable cyclotron oscillations in a cylindrical plasma shell, Phys. Fluids 4, 1412 (November 1961).

2. R. Bartsch, S. M. Thesis, Department of Electrical Engineering, M. I. T., June 1964.

3. H. A. Haus and D. L. Bobroff, A Small Signal Power Theorem for Crossed Field Devices, Raytheon Company Internal Memorandum (unpublished).

4. W. P. Allis, S. J. Buchsbaum, and A. Bers, Waves in Anisotropic Plasmas (The M. I. T. Press, Cambridge, Mass., 1963).

G. ELECTRON CYCLOTRON RESONANCE DISCHARGE*

Since the last report,[1] the relaxation of the discharge has been studied over long periods of time. For these experiments the system was operated in the burst mode, wherein the 1-μsec pulse train of the microwave power pulse was gated on and off at intervals of ~1 second. The decays of plasma electron density and x-ray intensity were studied in the afterglow that occurred between bursts of microwave pulses.

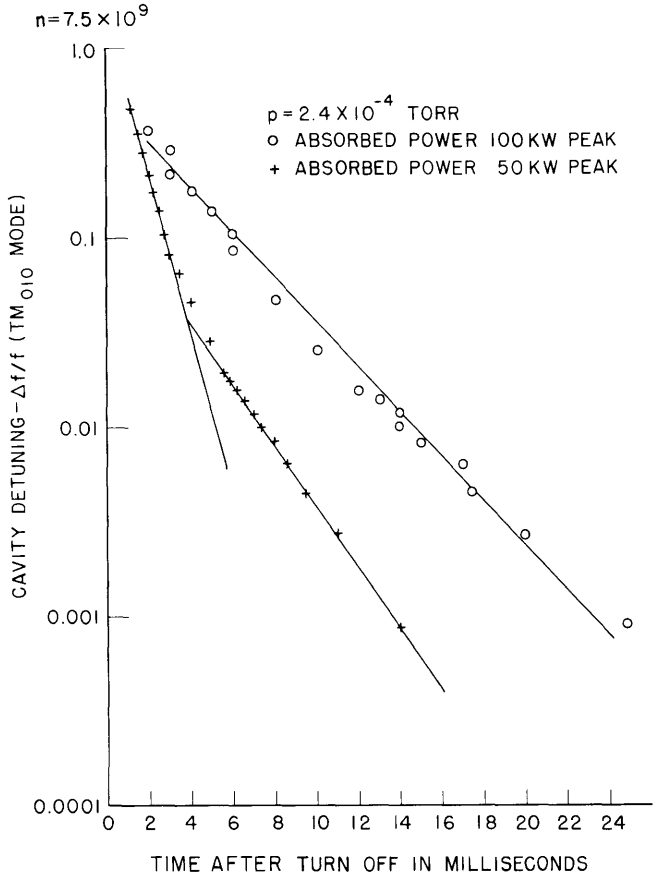

Fig. XV-17. Decays of electron density obtained from observing with the probing-mode technique at peak absorbed powers of 10 kw and 50 kw.

The plasma density decay was investigated with the use of the cavity-detuning technique of Rose and Brown[2]. The box in which the plasma is produced was excited near the resonance of the TM_{010} mode (545Mc). This mode, with E parallel to the magnetic axis, was chosen in order to minimize the interaction with the steady magnetic field. The detuning of the mode was measured by observing at what time in the afterglow the cavity was resonant at a given signal input frequency.

Figures XV-17 and XV-18 are graphs of the shift of the observed cavity resonant frequency as a funtion of time, after a burst of power pulses. According to the theory of Rose and Brown[2] the plasma electron density is proportional to $\Delta f/f$ (Δf is the resonant-frequency shift, and f is the unperturbed resonant frequency of the mode). Therefore, these curves show the decay of the electron density in the cavity. If one assumes that the plasma uniformly fills the cavity, then $\Delta f/f = 1$ implies a plasma electron density of $7.5 \pm 10^9/cm^3$.

*This work was supported in part by the United Stated Atomic Energy Commission under Contract AT(30-1)-3221.

Figure XV-17 shows the variation in the decay characteristics of the plasma electron density at a pressure of 2.4×10^{-4} torr in Hydrogen as the power absorbed by the discharge is varied. At the lower absorbed power one sees a decay composed of two exponentials. At the higher absorbed power the more rapid component of decay is absent.

Figure XV-18 shows the variation of the electron density decay characteristics with neutral pressure. The abscissa in these plots is the product of time and pressure. Of particular importance is the fact that over two orders of magnitude in pressure the points all fall on straight lines on a logarithmic plot, and with the exception of $p = 1.2 \times 10^{-4}$ the slopes of these lines are nearly equal.

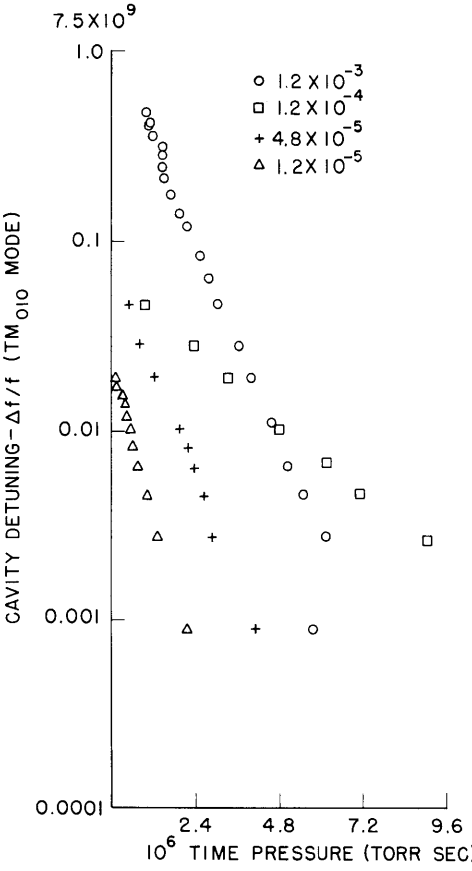

Fig. XV-18. Decays of electron density obtained from observing with the probing-mode technique at 83-kw peak incident power and magnet current of 50 amps.

It was impossible to investigate the electron density decay as a function of time for time less than the interval between microwave pulses (1msec). At higher pressures where the discharge is relatively stable, the electron density is too large ($\omega_p > \omega$) to be measured with this probing mode technique. At lower pressures the discharge is very unstable between pulses, and meaningful measurements are difficult to obtain.

Figure XV-19 shows decays of x-ray intensity with time after bursts of microwave power pulses. These curves were taken with the use of a sodium iodide scintillator and an RIDL pulse-height analyser operated in the multiscaling mode.

Figure XV-20 shows how the decay time constant τ multiplied by pressure p varies with pressure. The circles represent values of the parameter τp obtained with the probing-mode technique, and the crosses represent the decay time constant measured with the x-ray scintillator technique. Notice that the agreement between the two techniques is quite good and that both measurements show that the parameter τp is not a strong function of pressure.

The plasma decay as measured by these techniques can be explained quite satisfactorily as being due to collisions of the energetic electrons with neutral particles. After many collisions with the neutral particles, electrons are scattered into the escape cone

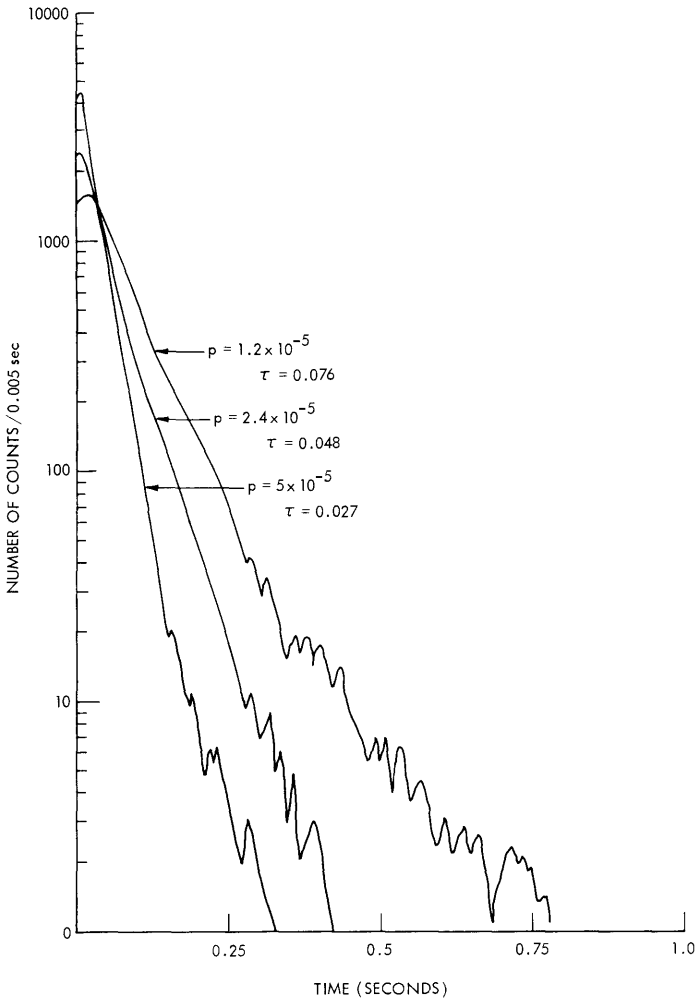

Fig. XV-19. X-ray decays at 80-kw peak incident power and magnet current of 60 amps.

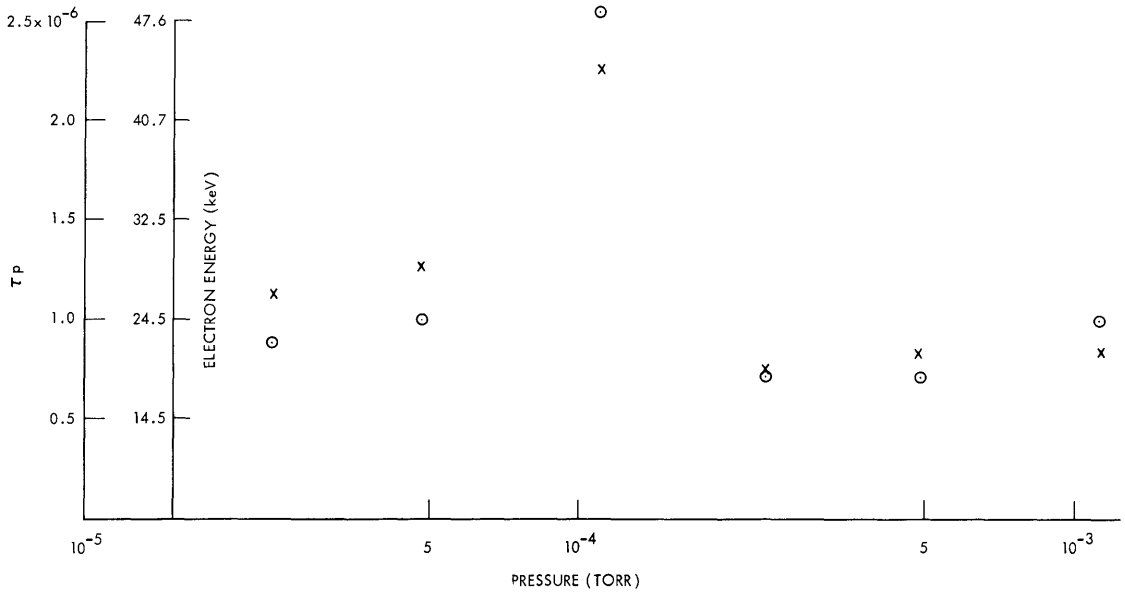

Fig. XV-20. Variation of the parameter -p with pressure and electron energies calculated from these values.

of the magnetic-mirror field and lost from the discharge. Collisions between charged particles are negligible a few milliseconds after the last microwave pulse because by this time the plasma density is several orders of magnitude less than the neutral density.

From the theory[3] of multiple small-angle scattering of electrons by neutrals, one can find a relation for the characteristic time (τ) required for an electron moving in a mirror field to be scattered into the escape cone of the mirror. One finds for hydrogen

$$\tau = \frac{3.14 \times 10^{-8} \theta^2 T^{3/2}}{p(1 + 0.278 \ln T)} \qquad (1)$$

where θ is the escape angle of the mirror field, and T is the electron energy in deV.

This relation shows that, if the electron energy T is a constant, the parameter τp will also remain constant. In the interpretation of the data presented in Fig. XV-20, we see that if we assume that the variation of T accounts for the fact the τp is not strictly constant, we find good agreement with the conclusion derived form Eq. 1. The electron energies indicated in Fig. XV-20 were calculated from Eq. 1. Those energies are in good agreement with electron energies obtained form the Bremsstrahlung spectra by the procedure outlined in the last report 1; Thus, for this experiment, we conclude that neutral scattering of electrons into the mirror loss cone accounts for the principal plasma loss mechanism after approximately the first millisecond of the afterglow.

T. J. Fessenden

References

1. T. J. Fessenden, Electron cyclotron resonance discharge, Quarterly Progress Report No. 75, Research Laboratory of Electronics, October 15, 1964, pp. 66-68.

2. D. J. Rose and S. C. Brown, J. Appl. Phys. 23,1028-1032(1952).

3. E. Fermi, Nuclear Physics (University of Chicago Press, Chicago (1950), p. 37.

H. THE HOLLOW-CATHODE DISCHARGE AS A LASER

It has often been suggested that the hollow-cathode discharge plasma[1] might be a suitable medium for a high-pressure cw laser. In the course of another experiment, an HCD plasma generator with a visually unobstructed central axis became available and was fitted with suitable optical devices to test for lasing action (see Fig. XV-21).

The mirrors (1 meter confocal, 98 per cent and 99.7 per cent peak reflectivity) were coated for maximum reflectivity at 4880 Å and had a bandwidth of several hundred angstroms. Tne reflectivity peak is at the wavelength of the very low-threshold Argon laser transition described by Gordon, Lasuda, and Bridges[2], and by Bennett and his coworkers.[3] The quartz Brewster angle windows were aligned within a degree or so, and the mirrors were adjusted so that the image of a filament held at one mirror was reflected back on itself by the other mirror. This procedure is known to be adequate for reasonably high-gain systems.

Tantalum cathodes of 0.125 inch and 0.188 inch O.D. were used, both with 0.010 inch wall thickness. The arc current was varied between 3 amps and 50 amps, and background pressure was adjusted over the range 5×10^{-4} - 2×10^{-1} torr. The background pressure was varied by both changing the gas feed rate and throttling the diffusion pump. No laser action was observed over the entire range of operating conditions. A scanning monochromator placed behind the 98 per cent reflective mirror showed no significant optical gain for any line within the reflectivity peak of the mirrors.

The 4880 Å line arises from the $4_p\,^4D_{1/2} \rightarrow 4s^2P_{3/2}$ transition of the Ar^+ ion. The upper level is thought to be pumped by direct electronic excitation from the neutral atom ground state. This process, requiring 35.5 ev electrons, is consonant with the observed

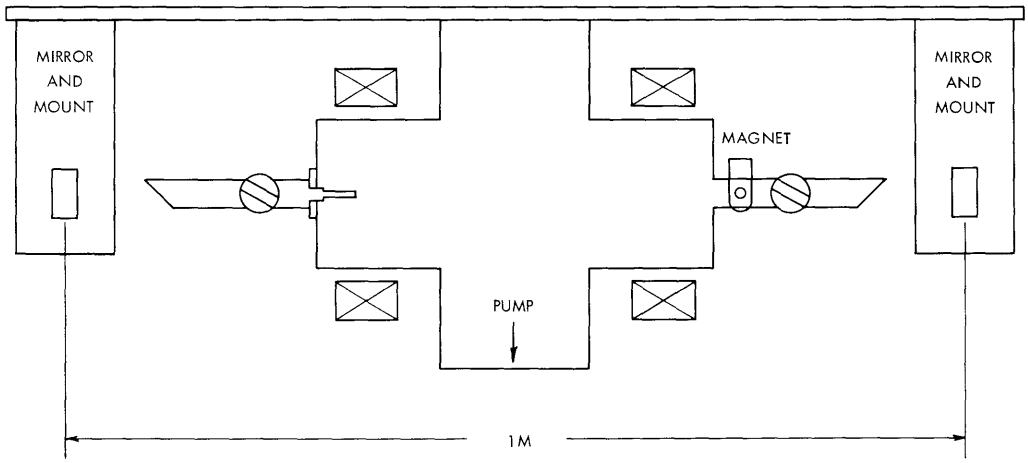

Fig. XV-21. Diagram of test conditions.

pressure and voltage gradient in Argon lasers. The inversion is aided, in the usual capillary arc, by the Doppler shifting of the $4s^2P_{3/2}$ level away from the frequency of its resonance radiation. The failure of the HCD to lase may therefore be due to short active length, to the low electric fields in the cathode interior, or to having too small a sheath drop to supply the necessary fast electrons. Another possible reason for lack of "lasing" action is wave front distortion by the turbulent gas behind the cathode. This was checked by telescopic observation of a glowing filament along the axis of an operating discharge. There was no noticeable deterioration of image quality. This, of course, is a necessary but not conclusive test of the optical path. The experiment is being continued in a system designed to minimize some of the difficulties noted here.

The mirror and mirror mounts were loaned to us by Dr. R. Carbone of Lincoln Laboratory, M. I. T.

P. H. Edmonds, E. T. Gerry, L. M. Lidsky

References

1. L. M. Lidsky, S. D. Rothleder, D. J. Rose and S. Yoshikawa, J. Appl. Phys. 33, 2490 (1962).

2. E. I. Gordon, E. F. Labuda, and W. B. Bridges, Appl. Phys. Letters 4, 178 (15 May 1964).

3. W. R. Bennett, Jr., J. W. Knutson, Jr., G. N. Mercer, and J. L. Detch, Appl. Phys. Letters 4, 180 (15 May 1964).

I. HOLLOW-CATHODE DISCHARGE III EXPERIMENT

The plasma produced in a hollow-cathode discharge exhibits a variety of interesting behaviors. Typical properties of such a plasma are $n_e \approx n_i = 10^{14}$/cc in the arc and 10^{12}/cc in the surrounding diffused plasma. Electron temperature of a few electron volts is approximately Maxwellian in the diffused plasma, but strongly anisotropic with streaming electrons in the arc.

Previous studies by Rothleder[1] indicated that under rather stringent operating conditions (gas feed $\approx$ 1 atm cc/sec., magnetic field $\approx$ 1 kgauss, background pressure $\approx$ 1 μ Hg, current of 40 amps in an arc of ~50-cm length), the plasma is apparently quiescent and describable by the linearized magnetohydrodynamic equations with transport coefficients derived from binary collision theory.

When these conditions are not met, the plasma is highly turbulent and dominated by rotating plasma spokes in the $E \times B$ direction. This phenomenon is characteristic of many arc plasmas. The frequency and amplitude of these oscillations depend on the operating parameters, but not in any obviously consistent manner. Morse[2] has studied this oscillation in detail in a weakly ionized (5 per cent) external plasma produced by an 8-inch Argon arc.

The geometry of previous experiments severely limited examination of the general

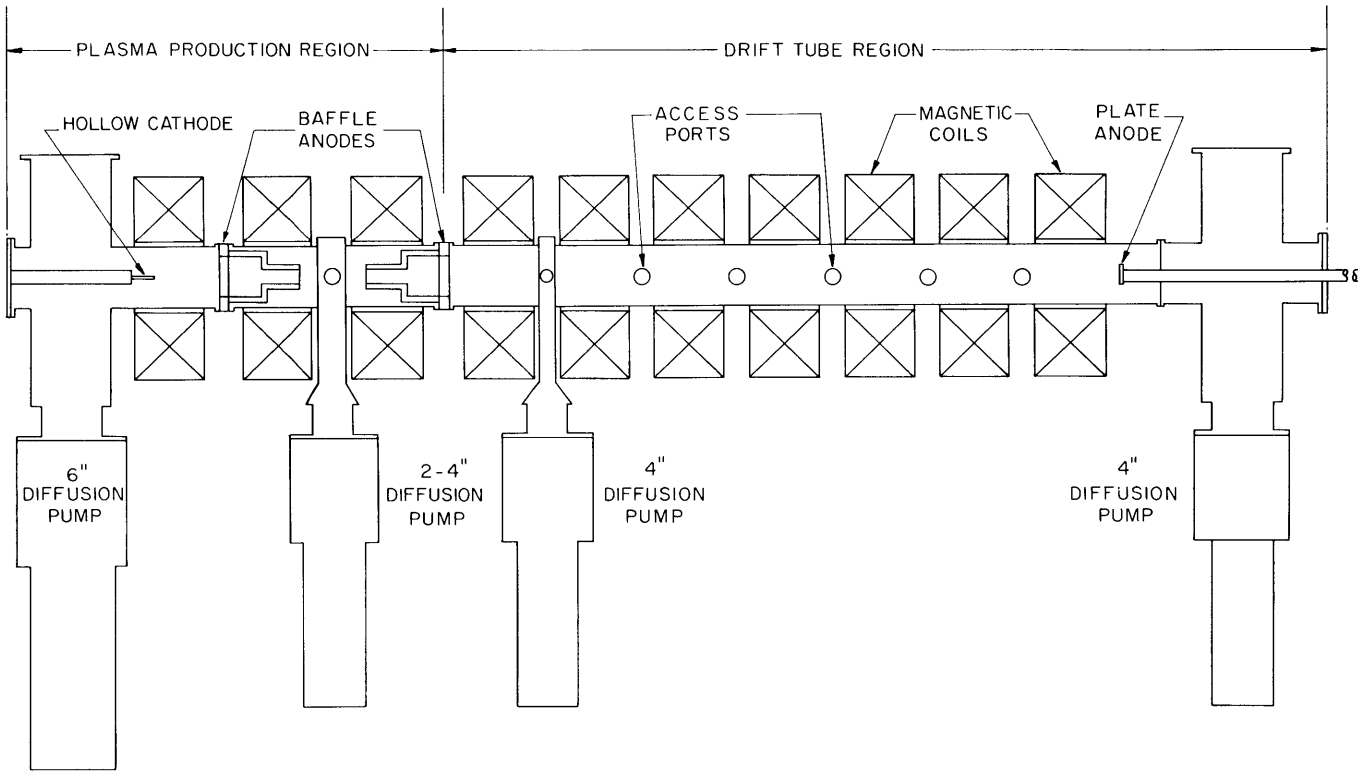

Fig. XV-22. Diagram of HCD III experiment.

validity of the theories. To study these phenomena more broadly, we are constructing an experimental apparatus that is sufficiently variable. By observing the phenomena under many different conditions, we expect to separate general phenomena from effects arising from peculiar and specific experimental conditions. The conceived system is shown schematically in Fig. XV-22. Basically, it is similar to the two-meter experiment described by Lidsky,[3] but utilizes a stainless-steel vacuum can instead of Pyrex tubes. It has increased axial length, magnetic field, diagnostic accessibility, and pumping speed.

1. Vacuum System

The vacuum system is made of 1/8 inch wall stainless-steel tubes. The entire system is 12 ft long and consists of two regions: a plasma-production region extending 3 1/2 ft, and a drift-tube region for plasma studies occupying the rest of the length. The plasma-production region is double-baffled for three-region differential pumping. Gas is fed through the hollow cathode, and excess gas is pumped by a 6-inch diffusion pump. Each baffle has a maximum conductance of 40 liters/sec and may be reduced by inserts. The baffles are electrically insulated from the rest of the system; thus, the first may be an anode, and the second may be biased to draw electrons and hence vary the space potential. The region between the two baffles is pumped by two 4-inch diffusion pumps.

In order to fully utilize the pumping speed, the vacuum chamber is brought out to narrow rectangular boxes that match the pumping area of the pumps. Two more 4-inch diffusion pumps are located at the two ends of the drift tube. The pumping speed in this region is basically limited by the conductance of the drift tube itself. With gas feed of 1 atm-cc/sec, the pressure in the drift tube will be $\approx 10^{-6}$ torr; for a plasma density of 10^{12}/cc, the degree of ionization will be ≥ 96 per cent and may be further increased by limiting baffle conductance.

The degree of ionization may also be varied by introducing a variable leak into the drift tube. The tube proper is 6 ft fong, and has axial access at 9-inch intervals and aximuthal access at angles of 45°, 90°, and 180°. A piston-type plate anode that slides through an O-ring seal, is located at the extreme end to permit variation of the length of the discharge. The vacuum system is now being assembled. Figure XV-23 is a photograph of the present stage.

2. Magnets

The magnetic field will be generated by 10 coils, three of which are used in the plasma-production region, energized by a 15-kw arc welder supply. The seven remaining coils will be used in the drift region, spaced at 2-inch intervals where the field ripple should be less than 7 percent. By proper shimming, the ripple should be less than 1 per cent; thus, any plasma phenomena associated with curvature of the field

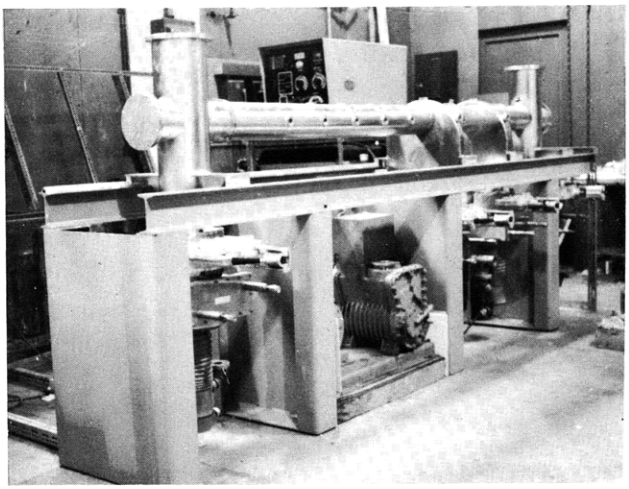

Fig. XV-23. Photograph of the present vacuum system.

lines, will be eliminated. Each coil measures 7 inches I.D., 20 7/8 inches O.D., and 7 inches wide, and consists of two tape-wound pancakes separated by a cooling pancake. The magnet coils are designed to take 9 kw each, requiring 2 gpm water cooling and producing a field of 3.1 kgauss. Because of available power in the laboratory, the coils will normally be operated only at 7 kw. The excess capacity permits extensive field shaping – for example, into radial minimum or maximum field configurations. These shapes have an important effect upon the arc stability.[4]

3. Modes of Operation

The system can be operated in several configurations. For example, in the arc mode the discharge is run between the hollow cathode and the plate anode. Here the plasma is expected to be vulnerable to instabilities driven by longitudinal currents. In the reflex mode, the arc runs between the cathode and the first-baffle anode; thus the drift-tube region is free from longitudinal electric field. The plasma can then be examined for weakly unstable modes driven by the radial density gradient.

J. C. Woo, L. M. Lidsky, D. J. Rose

References

1. S. Rothleder, Ph.D. thesis, Department of Nuclear Engineering, M.I.T., 1962.

2. D. L. Morse, Ph.D. thesis, Department of Electrical Engineering, M.I.T., 1963.

3. L. Lidsky, Quarterly Progress Report No. 63, Research Laboratory of Electronics, M.I.T., October 15, 1961, pp. 33-40.

4. R. A. Gibbons (paper to be published in Phys. Rev. Letters).

J. ARGON EXCITED-STATE DENSITIES IN A HOLLOW-CATHODE DISCHARGE*

1. Introduction

The interaction of laser beams with partially ionized plasmas in many cases is very strongly affected by photo-ionization of excited neutral atoms in the plasma. The ionization rate is very sensitive to the density of the lower ionizable levels ($p \geq 3$ for hydrogenic atoms and 6934 Å radiation) because the photoionization cross section varies as p^{-5}, where p is the principal quantum number. The lower states, however, with their short radiative lifetimes are usually very far from Saha-Boltzmann equilibrium in laboratory plasmas; thus there is no simple way to compute their population densities. McWhirter and Hearn[1] have recently published the results of calculations predicting the lefel densities as functions of neutral or ion ground-state densities, and electron temperature. The experimental work reported here, a partial verification of their results, indicates that the excited level densities may be predicted with reasonable (factor of 2-3) accuracy.

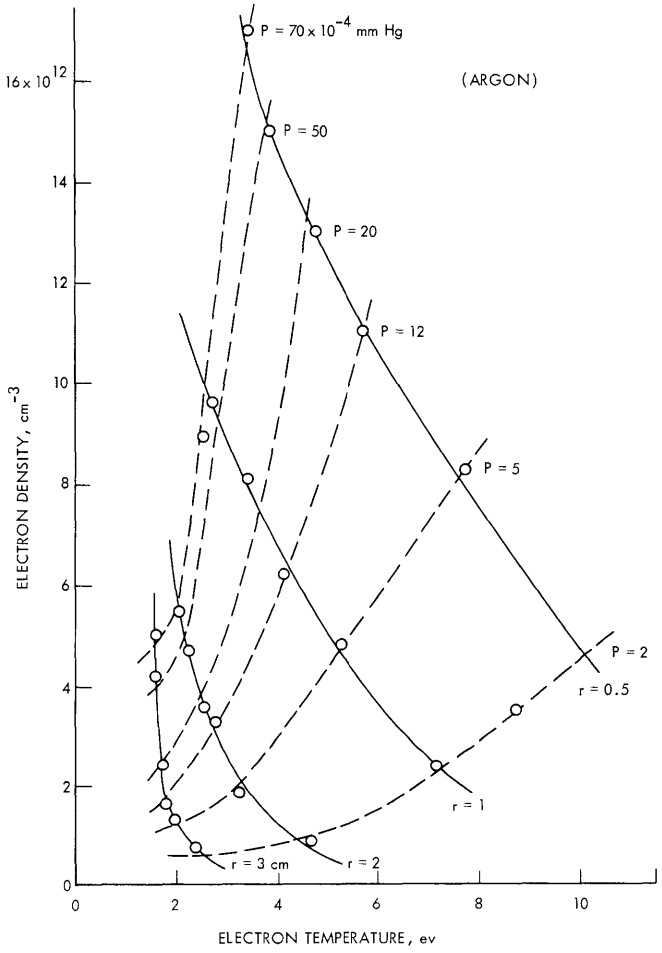

Fig. XV-24. Variation of electron density and temperature with background pressure and distance from the center of the arc.

2. Experiment

The plasma used for these experiments was created by a differentially pumped hollow-cathode discharge. The steady-state plasmas had density of $10^{13}/cm^3$, $T_e \sim 4$ ev, and fractional ionization of approximately 60 per cent. Representative plots of the variation of plasma properties with radius at constant pressure and with pressure at fixed radius, as

*This work was supported in part by the United States Atomic Energy Commission under Contract AT(30-1)-3221.

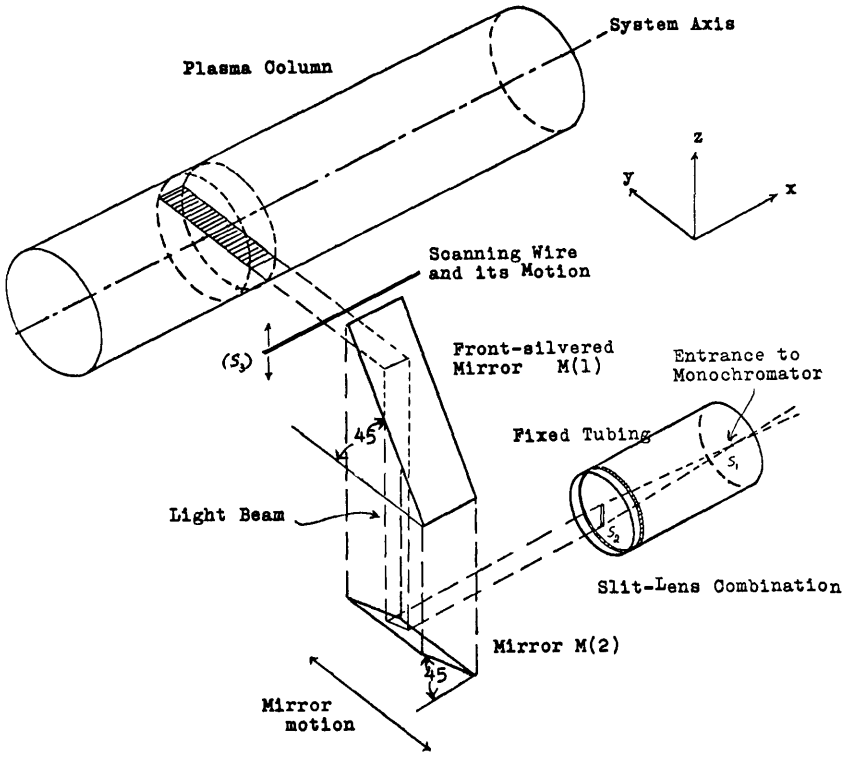

(a)

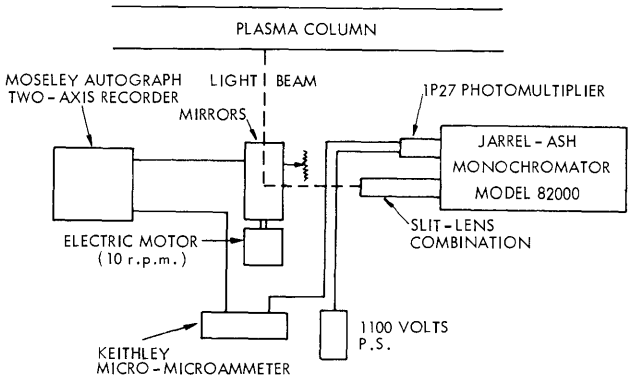

(b)

Fig. XV-25. (a) The optical system. (b) Experimental arrangement.

measured by Langmuir probes, are shown in Fig. XV-24.

The excited-state densities were obtained by measurement of line radiation intensities. The detection and recording systems are diagrammed in Fig. XV-25 with typical recorder output shown in Fig. XV-26. The spatial resolution was 1 × 15 mm with the large dimension parallel to the discharge axis. The spectral resolution was 0.2 Å. The entire optical chain was calibrated against a standard ribbon filament lamp placed at the position of the discharge axis.

Photomultiplier current readings, $I_{pi}(z)$, were converted to spatially resolved excited excited-state densities through the equation

$$q_{pi}(r) = \frac{-2}{\pi a A_{pq} \eta^*} \sum_{z=r}^{N} B_{rz} I_{pi}(z), \tag{1}$$

where the B_{rz} are the Abel transform coefficients for converting the line intensities (measured along transverse sections of the plasma) to the desired radial variation[2]; N is the number of zones, each of width a, into which the plasma column was divided for the

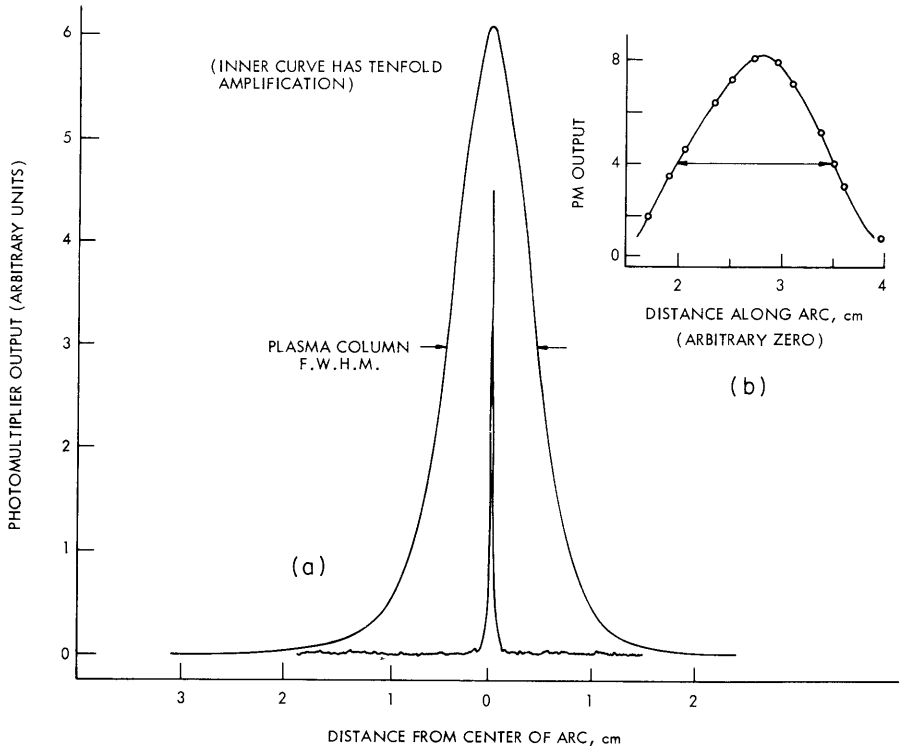

Fig. XV-26. (a) Typical plasma column profile with superposed vertical resolution of the optical system. (b) Horizontal resolution.

Abel transform; A_{pq} is the transition probability from level pi to lower level qj,[3] and η^* is the efficiency of the optical system.

The Abel inversion was performed with an error of < 1.5 per cent. We estimate that the total experimental error in measurement of absolute excited-state densities is less than 15 per cent.

3. Experimental Results and Theoretical Prediction

McWhirter and Hearn present their results in terms of two coefficients, $r_p(0)$, and $r_p(1)$, representing the linear dependence of the population density, q_p, of level p to the ground-state density q_1 by

$$q_p = q_{pE}\{r_p(0) + r_p(1)\,(q_1/q_{1E})\}, \tag{2}$$

where the subscript E denotes the Saha-Boltzmann equilibrium characterized by

$$q_{pE} = \frac{q_e^2}{X}\, p^2 \left[\frac{h^2}{2\pi m k T_e}\right]^{3/2} \exp\left(\frac{W^* - W_p}{kT_e}\right). \tag{3}$$

Here, q_e and T_e are the electron density and temperature, X is the ratio of free electrons to ions, W_p is the level energy, and W^* is the ionization potential.

The population of the entire p^{th} level is represented by q_p. To extend this to allow comparison with the measured sublevel densities, we make use of the experimental result that the sublevel populations for low p may be characterized by a measured excitation temperature that remains constant with changes in position or ground-state density. (Constancy, for instance, of the ratio of the population densities of the two levels shown in Figs. XV-27 and XV-28 supports this statement.) By using this excitation temperature, Ta, (equal to 1.7 ev for Argon), Eq. 2 becomes

$$q_{pr} = q_{10} r_p(1)(g_{pr}/g_{po})(1+Q)\, p^2 \exp\left\{\frac{W_{po} - W_{pr}}{kT_a} - \frac{W_{po}}{kT_e}\right\}, \tag{4}$$

where the second subscript refers to the individual sublevels, g_{pi} is the statistical weight of the i^{th} sublevel of the state whose principal quantum number is p, and

$$Q = \left[\frac{h^2}{2\pi m k T_e}\right]^{3/2} \cdot \frac{q_e^2}{X q_{10}} \cdot \frac{r_p(0)}{r_p(1)} \exp\,(W^*/kT_e). \tag{5}$$

Physically, Q stands for the ratio of populating the pr^{th} sublevel from above and below, three-body recombination and direct excitation from the ground state being by far the dominant processes in our case. For the plasmas under consideration, Q is of the

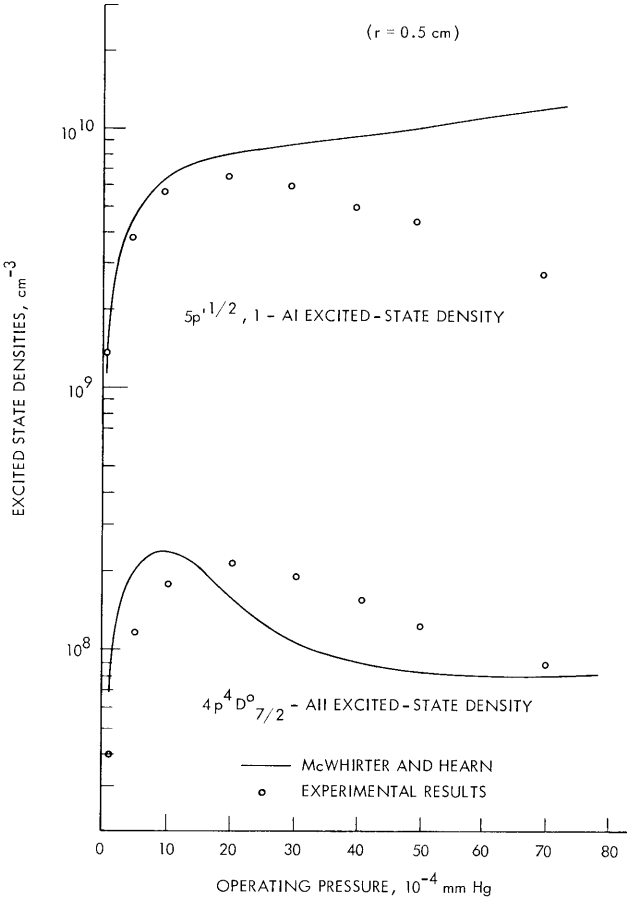

Fig. XV-27. Variation of two Argon excited-state population densities with background pressure at constant radius.

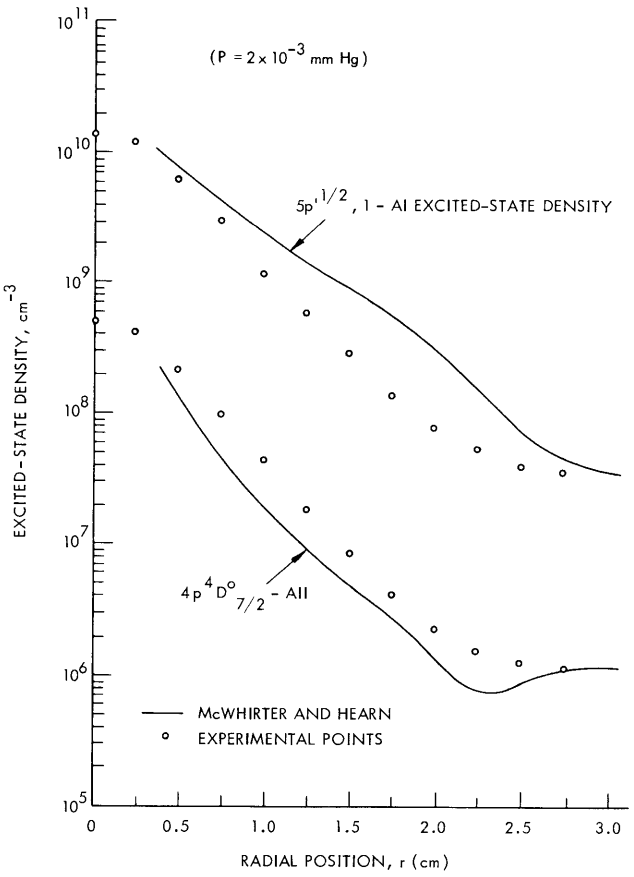

Fig. XV-28. Radial variation of two Argon exc state densities with constant backgr pressure.

order of 10^{-2}-10^{-3} for the lower levels, and reflects the much higher than equilibrium concentration of neutrals flooding the system through the cathode. It becomes relatively significant only for very low temperatures, and hence outside the main plasma core. Its sole effect on the population densities examined here appears in the AII case for $r > 2$ cm.

The measured excited-state densities are compared with those predicted by Eq. 4 in Figs. XV-27 and XV-28. We have assumed that the low-lying levels may be treated as hydrogenic states. The only major (order-of-magnitude) discrepancy occurs at relatively high pressures where it is likely that the high-energy tail of the electron distribution is depleted.

Further details concerning this work will be found in J. N. Hamawi's thesis.[4]

J. N. Hamawi, L. M. Lidsky

References

1. R. W. P. McWhirter and A. G. Hearn, Proc. Phy. Soc. (London) 82, 641 (1963).

2. O. H. Nestor and H. N. Olsen, SIAM Review Vol. 2, No. 3. p. 200, 1960.

3. B. D. Adcock and W. E. G. Plumtree, J. Quant. Spec. Rad. Trans., Vol. 4, No. 1, p. 29, 1964.

4. J. N. Hamawi, S.M. Thesis, Department of Nuclear Engineering, M.I.T., 1964.